CrossMark

ORIGINAL PAPER

Landslide hazard mapping in the Constantine city, Northeast Algeria using frequency ratio, weighting factor, logistic regression, weights of evidence, and analytical hierarchy process methods

Hamid Bourenane[1,2] · Mohamed Said Guettouche[1] · Youcef Bouhadad[1,2] ·
Massinissa Braham[1,2]

Abstract Landslides constitute the most widespread and damaging natural hazards in the Constantine city. They represent a significant constraint to development and urban planning. In order to reduce the risk related to potential landslide, there is a need to develop a comprehensive landslide hazard map (LHM) of the area for an efficient disaster management and for planning development activities. The purpose of this research is to prepare and compare the LHMs of the Constantine city, by applying frequency ratio (FR), weighting factor (Wf), logistic regression (LR), weights of evidence (WOE), and analytical hierarchy process (AHP) methods used in a framework of the geographical information system (GIS). Firstly, a landslide inventory map has been prepared based on the interpretation of aerial photographs, high resolution satellite images, fieldwork, and available literature. Secondly, eight landslide-conditioning factors such as lithology, slope, exposure, rainfall, land use, distance to drainage, distance to road, and distance to fault have been considered to establish LHMs using the FR, Wf, LR, WOE, and AHP models in GIS. For verification, the obtained LHMs have been validated comparing the LHMs with the known landslide locations using the receiver operating characteristics curves (ROC). The validated results indicate that the FR method provides more accurate prediction (86.59 %) of LHMs than the WOE (82.38 %), AHP (77.86 %), Wf (77.58 %), and LR (70.45 %) models.

On the other hand, the obtained results showed that all the used models in this study provided a good accuracy in predicting landslide hazard in Constantine city. The established maps can be used as useful tools for risk prevention and land use planning in the Constantine region.

Introduction

Landslides constitute the most frequent and damaging natural hazards threatening the human lives and properties in northern part of Algeria. The landslide incidences in a region have been of serious concern to the society due to the loss of life, natural resources, infrastructural facilities, and also posing problem for future urban development. The city of Constantine in northeast, which is the third largest city of Algeria, suffered from extensive and severe landslides causing serious damages to property and infrastructure (Machane et al. 2008; Guemache et al. 2011; Bourenane et al. 2014). The most recent landslides that occurred in 2002, 2003, 2004, 2006, and 2012 have caused substantial damage to several buildings and major infrastructures (such as the Sid Rached bridge, Ciloc buildings, Rhumel bridge, Mentouri university, Boussouf district, Benchargui district, Boudraa Salah district, the national road number 27, etc.). These landslides have alerted the authorities towards the seriousness of landslide management and prevention. However, there has been too little consideration of potential problems in land use planning and slope management. Recently, the Algerian authorities have been stressing the need for local planning authorities to take landslides into

✉ Hamid Bourenane
b.hamid@hotmail.com

[1] USTHB, University of Science and Technology Houari Boumediene Bab Ezzouar, El Alia, Algiers, Algeria

[2] CGS, National Center of Applied Research in Earthquake Engineering, 1 Rue Kadour Rahim, Hussein-Dey, Algiers, Algeria

Springer

account at all stages of the landslide hazard mapping process. So far, few efforts have been made to predict or prevent these events which caused serious damages. Nowadays, the landslide disaster situation is further compounded by increased vulnerabilities related to rapidly growing population, unplanned urbanization, rapid development in high-risk areas, environmental degradation, and climatic change with the heavy rainfall. Landslide disasters also become the major obstacle in development process because their economic losses are relatively high.

Through scientific analysis, the landslide hazard map is of crucial importance in the economic planning of urban areas and engineering structures (Ercanoglu and Gokceoglu 2002). Therefore, the preparation of landslide hazard mapping is a basic tool for disaster management and planning development activities in urban and rural areas. The result of landslide research may provide valuable information that helps to forecast such events as well as to find measures to mitigate subsequent losses to future landslides.

Landslide hazard (LH) is defined as the probability of occurrence of landslides in a given area within a reference period of time (Varnes 1984). Landslide hazard mapping is associated to the division of area in homogenous zones and their ranking according to degrees of landslide hazard. LH is deduced from two aspects: (i) landslide susceptibility expressing the spatial probability of occurrence of a landslide for given predisposing terrain factors (lithology, slope, land use, etc.) in a given area (Brabb 1984; Crozier and Glade 2005) and (ii) the temporal dimension of landslides related to the occurrence of triggering events (rainfalls, earthquakes, etc.). However, LH is, often, restricted to landslide susceptibility and did not refer to the time occurrence of landslides because of the absence of historical landslide records. Consequently, most of the published hazard maps have only presented the spatial information of landslide hazard and did not refer to the time dimension of landslides.

The aim of this research is to present and compare detailed landslide hazard maps (LHMs) for the Constantine city (northeast of Algeria), using frequency ratio (FR), weighting factor (Wf), logistic regression (LR), weights of evidence (WOE), and analytical hierarchy process (AHP) methods in the framework of GIS. These models are tested, and the obtained results have been discussed. The results provide useful information about landslide risk mitigation and may serve as guidelines for land use planning in Constantine city.

The present paper is organized into four parts. The first part describes the landslide phenomena in the Constantine city and includes a related literature review of achieved works prior to this research; the second part presents the prepared landslide database; the third part describes the application of two statistical approaches, namely, the bivariate and multivariate with an expert knowledge-based model (AHP) for landslide hazard mapping in the studied area and, finally, the fourth part provides the validation and comparisons of the obtained LHMs.

Scientific literature review

A wide variety of methods and techniques for landslide hazard mapping have been developed and applied in literature, including qualitative and quantitative methods (Soeters and Van Westen 1996; Leroi 1996; Guzzetti et al. 1999; Aleotti and Chowdhury 1999; Van Westen et al. 2003; Dai et al. 2001). Recently, several attempts have been made to apply different methods of LHM and to compare results searching for the best suited model.

Qualitative methods are subjective, based on expert knowledge, and portray hazard zoning in descriptive terms. These methods can be classified into two groups. The first group is base on the geomorphologic analysis where the landslide hazard is determined directly using experiences and knowledge of experts; a direct relationship between existing landslides and causative terrain parameters is determined and used to construct landslide hazard. The second group is a qualitative map combination where a landslide hazard map is obtained by combining a number of landslide influence factor maps. The weights are assigned to subclasses of thematic maps based on the field knowledge of experts; therefore, a landslide inventory map is not needed. Moreover, there are qualitative methodologies which use weighting and rating procedures known as semi-quantitative methods. These methods are the analytic hierarchy process (AHP) (Saaty 1980; Barredo et al. 2000; Yalcin 2008) and the weighted linear combination (WLC) (Ayalew and Yamagishi 2005). The AHP method involves the creation of hierarchy of decision elements (factors) and the comparison between different pairs of elements in order to assign a weight and a consistency ratio for each element. While WLC approach is a concept which combines maps of landslide-controlling parameters, by applying a standardized score (primary-level weight) to each class of a certain parameter and a factor weight (secondary-level weight) to the parameters themselves. Although, results of these approaches are partly subjective, depending on the expert knowledge (Van Westen et al. 1997; Leroi 1996). The qualitative or semi-quantitative methods have proved their utility in the case of regional studies (Soeters and Van Westen 1996; Guzzetti et al. 1999).

Quantitative methods are based on numerical expressions of the relationship between causal factors and the landslides. The main concept of the indirect approaches is that the controlling factors of future landslides are the same as those observed in the past (Carrara et al. 1995). Two types of quantitative methods can be distinguished: deterministic and statistical (Aleotti and Chowdhury 1999). Deterministic methods are focuses on the analysis of the mechanical equilibrium of a

potential slide block and calculate the slope safety factor (Zhou et al. 2003). Due to the need of exhaustive data from individual slopes, these methods are often effective to map only small areas. Statistical methods are based on the analysis of the functional relationships between landslide-controlling factors and the distribution of landslides. The statistical methods include the bivariate statistical models, the multivariate, the logistic regression, the fuzzy logic, the artificial neural network analysis, etc. These methods are formally very rigorous because they consider the interrelationships among the different causal factors.

Statistical methods are considered by the scientific community as more objective and more suitable for susceptibility and hazard mapping at medium and large scale (1:50.000, 1:25, 000, and 1:10.000) because of their potential to minimize the expert subjectivity (Soeters and Van Westen 1996; Van Westen et al. 1997; Van den Eeckhaut et al. 2006; Thiery et al. 2007).

The statistical methods require the collection of a large amount of data in order to produce reliable results. Moreover, the geographic information system (GIS) is a valuable tool used to collect, to store, to process, manipulate, and to correlate the large amounts of data in order to build landslide hazard maps. Thus, GIS constitute a basic tool for landslide hazard mapping due to its efficiency in spatial data management, manipulation, and spatial analysis which allow the update of the hazard assessment procedures.

Geographical, geomorphological, and geological setting of the study area

The Constantine city is located in northeast of Algeria, at about 430 km east of the capital city of Algiers (Fig. 1). The study area concerns the master plan city perimeter that covers about 60 km^2. The city of Constantine is highly affected by landslide hazards, due to its geomorphological, geological, climatic, and seismotectonic conditions, as well as the anthropogenic factors.

Geomorphologically, the Constantine area belongs to the northeast mountainous area of the Tellean Atlas, which is characterized by contrasting relief that combines mountains, plates, hills, and river plains. The altitude ranges from 300 to 1000 m and decreases from Northeast to Southwest. The

Fig. 1 Geographical location and Digital Elevation Model (DEM) of the study area
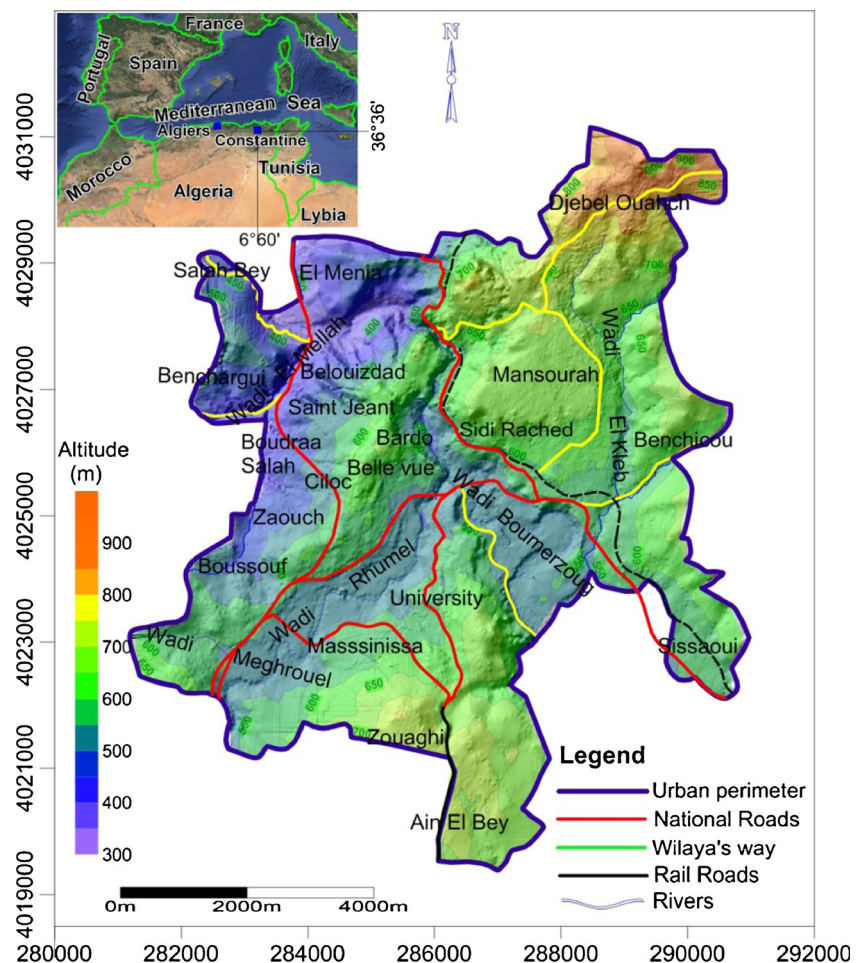
hydrographic network is represented by two main rivers (Rhumel and Boumerzoug) with a permanent flow that are associated with the Mellah, Megharouel, and Chaabet El Klab rivers having temporary flow (Fig. 1).

Geologically, the Constantine region belongs to the external domain of the Tellean Atlas chain, a part of the North African Alps (Maghrebides), built during the main paroxysmal compressional phases of Eocene, Miocene, and Quaternary periods (Vila 1980; Letouzey and Tremolieres 1980). Lithologically, the studied area presents four main sedimentary units: (i) the Cretaceous marls and limestone bed rock that belongs to the Constantine neritic formation; (ii) the Cretaceous-Eocene marls and calcareous marls of the Tellian thrust sheet unit; (iii) the Mio-Pliocene sandy clays, marls and conglomerates; and (iv) the Quaternary alluvial terraces and lacustrine calcareous formations (Guiraud 1973; Vila 1980; Aris et al. 1998; Benaissa and Bellouche 1999; Bougdal et al. 2006). The Neogene clays and the conglomerates formations, covering a large surface of the Constantine urban plan, are very sensitive to the presence of the water with average-to-high plasticity, and then, constitute prone zones to landsliding.

The climate of the Constantine region is semi-arid, with a typical hot and relatively dry season between June and August and a wet season during December to April. The rainy period corresponds to December, January, and February with the rainfall amount ranges between 350 and 500 mm. However, the rainfalls are concentrated in a short period as rainstorms and super rainstorms representing a major landslide hazard factor in the area.

The Constantine city is characterized by an important economic, scientific, and cultural infrastructures as well as high population density (2.374 inhabitants/km^2) (RGPH 2008). The city experienced significant urban changes during the different periods of its history; each period offers a particular developed urban area. Before and during the Ottoman period (prior to 1837), Constantine was built and limited to the stable bed rock. During the French period (1837–1962), the city expanded towards less stable zone. Since the Algerian independence (since 1962 up to now), the expansion of city has accelerated and unstable zones have been occurred. Since then, new settlements combined with inappropriate land use constitute the main factors of the increase of the frequency of landslides.

Spatial database construction using GIS

The first step for the production of LSM is data collection and construction of a spatial database from which the relevant landslide-conditioning factors have been extracted. A spatial database that considers the landslide-related factors is constructed for the study area. The reliability of LHMs depends, mostly, on the amount and the quality of the available data, the working scale, and the selection of the appropriate methodology of analysis and modeling.

Firstly, the landslide inventory map is prepared for the study area, based on the analysis of aerial photographs and satellite images, completed by field investigation. Secondly, eight possible causative factors such as lithology, slope, exposure, land use, rainfall, distance to stream, distance to road, and distance to fault have been identified, analyzed, and thematic layers have been derived and prepared from (Table 1): (i) the available

Table 1 Spatial database of the study area

Data layers	Source of database
Landslide inventory	Landslide inventory database, satellite imagery (Alsat 2A) at 1:10,000 scale, aerial photographs at 1:10,000 scale, Google Earth data, field surveys
Relief (slope and aspect)	DEM at 1:10,000 scale (10-m resolution) generated by digitization and interpolation of elevation lines extracted from topographic map at 1:10,000 scale from URBACO (centre d'études & réalisations en urbanisme de Constantine)
Geology	Geological maps at 1:10,000 scale, field survey, boreholes from geotechnical studies from DUC of Constantine (Direction de l'Urbanisme et de la construction)
Hydrology (distance to streams and rainfall)	Satellite imagery Alsat 2A at 1:10,000 scale (2.5 m resolution), aerial photographs at 1:10,000 scale, national topographic map at the scale of 1:25,000, field survey. Precipitation database covering a time period of 32 years from the 04 meteorological stations of the ANRH (National Agency of Meteorology and Hydrology) and the ONM (National Office of Meteorology)
Land use	Satellite imagery Alsat 2A, aerial photographs, Google Earth data, land use map at 1:10,000 scale (master city plan "PDAU") from DUC (Direction d'Urbanisme et de la Construction) and field survey
Distance to roads	Satellite imagery Alsat 2A, Google Earth data, aerial photographs, national topographic map at the scale of 1:25,000, field survey
Distance to faults	Geological maps at 1:50,000 and 10,000 scale, field survey

national databases, (ii) aerial photographs and satellite images analyses, and (iv) field surveys. The thematic layers generated in GIS software have been re-sampled in a 10 m×10 m grid size in order to facilitate the easy raster-based computation. All maps were geo-referenced in the local projection system of Algeria (UTM zone 32 WGS 84—Geodetic Reference System). The statistical treatment of the data has been performed by using Excel 2007 and Xl Stat 2014 trial version software.

Landslide characteristics and inventory map

The landslide inventory map is considered as the basis and the most fundamental step in landslide hazard mapping. Landslide inventory maps provide the spatial distribution of existing landslides and their properties. These maps can be prepared using different techniques depending on the scope of the work, the extent of the study area,

the scales of base maps, the quality and detail of the accessible information, and the available resources to carry out the work. The landslide inventory map of the study area (Fig. 3a) has been prepared at 1:10,000 scale, from the analysis and interpretation of aerial photographs, recent high resolution satellite images, field surveys, and available literature. Aerial photographs (Fig. 3d) were taken in 1980, at a scale of 1:10,000 by the National Institute of Cartography (INCT). Alsat 2A panchromatic satellite image (Fig. 3b) with spatial resolution of 2.5 m was taken in 2011 at a scale of 1:10,000. A satellite image of Google Earth (Fig. 3c) taken between 2003 and 2013 has been also used for visual detection of landslide occurrences in the study area.

In some cases, recent landslide locations have been identified from Alsat 2A satellite images and from Google Earth data. Field investigation has been conducted between 2008 and 2013 (Fig. 2) to verify and complete the photo

Fig. 2 Field photographs showing the characteristics and types of recently occurred landslides in the study area: **a** rotational slides over the road of Massinissa, **b** rotational slides in Boussouf, **c** rotational slides along road in Benchergui, **d** fall slides in Benchergui, **e** rotational slides in Chabet El Merdja, and **f** rotational slides of the Rhumel bridge in Massinissa
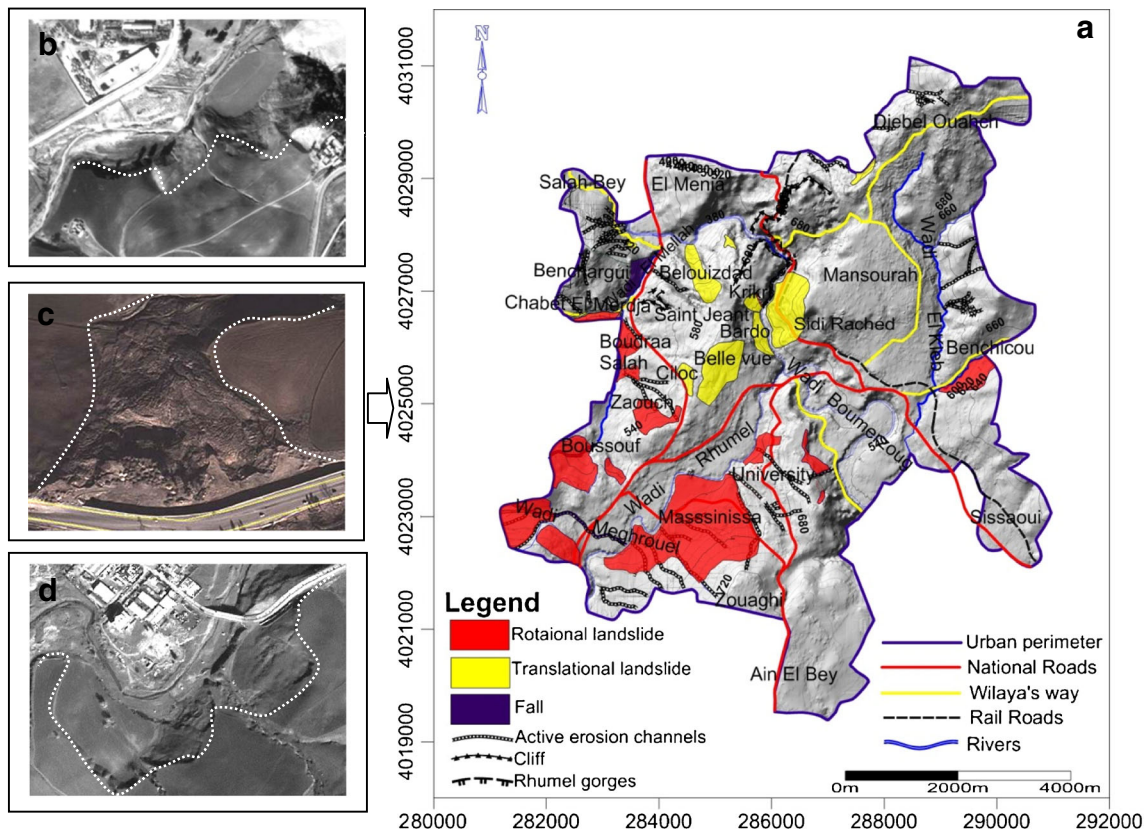
Fig. 3 **a** Landslide inventory map of the study area and examples of different types of optical remote sensing images used for determination of landslides in the Constantine city. **b** Section of an aerial photo at 1:10,000 scale taken in 2002. **c** Section of a satellite image of Google Earth. **d** Section of a satellite image (Alsat 2A) at a scale of 1:10,000 taken in 2012 (the *white dashed line* marks the scarp)

interpretation, check the sizes and shapes of landslides, identify the types of movements, the materials involved, and the activity of failed slopes. In addition, all the available literature including historical landslide reports, scientific publications, thesis, dissertations, and archives from local authorities have been gathered and examined in order to complete the landslide inventory map (Arcadis 2003; Bougdal 2007; Machane et al. 2008; Guemache et al. 2011). The landslide database is obtained by integrating the collected data and then imported into GIS to create the landslide inventory map at 1:10,000 scale. After that, the landslide vector map is transformed into a grid database at 10×10 m cell size. The geometrical (perimeter, area, and maximal length) and geomorphological characteristics (typology and state of activity) of landslides have been determined clearly and stored in a GIS database using Arc GIS 9.1 software.

The obtained landslides perimeter covers an area of 7.124 km^2 that represents 12 % of the total urban area. The most landslide-prone zones are located in the left bank of the Rhumel river and in the most urbanized zone of the Constantine city, as shown in Fig. 3a. An example of recent landslides identified in the study area and their morphological characteristics is shown in Fig. 2.

According to the landslide classification proposed by Varnes (1978), active landslides can be grouped into three main types: translational, rotational, and fall. The most failures (72 %) correspond to rotational debris slides, 26 % correspond to translational slides, and the remaining (2 %) are rockfalls. The rotational slides are located along streams but in more gentle slopes compared to the translational slides and occur mainly in Miocene marly clay deposits. The translational slides of variable sizes are located on steep slopes and affect the Miocene conglomerates and the Cretaceous marly-limestone of the Tellean thrust sheet. Mostly, the determined landslides had occurred as a result of heavy rainfalls. Landslide activity reaches its maximum during and just after rainy events. During the heavy rainfall of 2002–2003, 2003–2004, and 2005–2006 winters, the accumulated precipitation reached 460–800 mm and many landslides have been occurred and reactivated in the studied area (Chemin forestier, Chabet El Merdja - Sotraco-Boudraa Salah, Bardo, Poudriere, Boussouf, and Masssinissa). Besides, runoffs related to snow melting and rain as well as infiltrations in the schistose marl, favored by the high permeability of these fissured rocks, increase the interstitial pressure and make
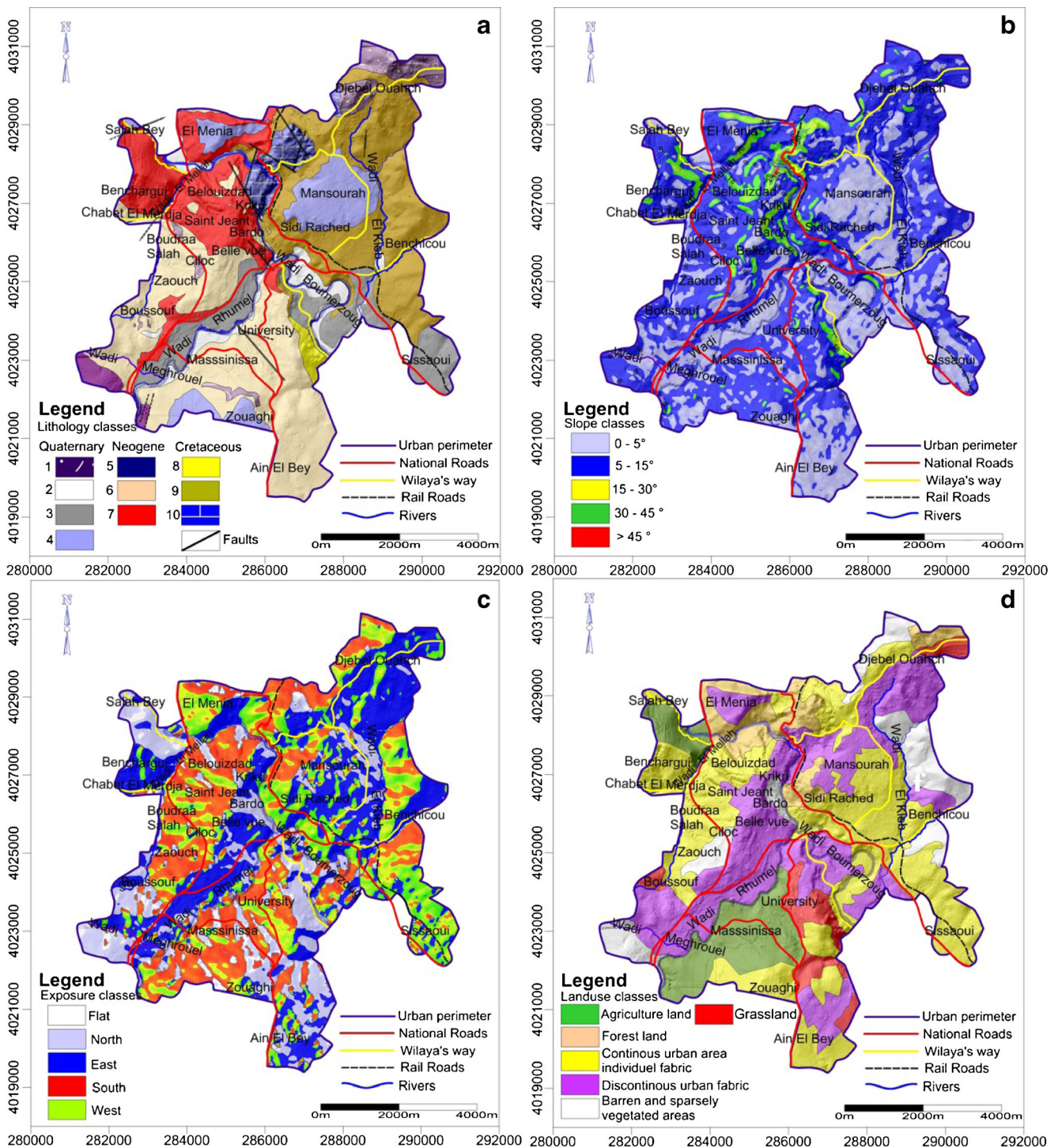
Fig. 4 Landslide-conditioning factors of the study area: **a** Lithological map. *Legend*: (*1*) *Quaternary Colluviums, conglomerate and Thick fill;* (*2*) *Quaternary recent alluvial terraces*; (*3*) *Quaternary ancient alluvial terraces*; (*4*) *Quaternary lacustrine limestones*); *5*) *Pliocene lacustrine limestones*; (*6*) *Miocene conglomerates*); (*7*) *Miocene marly clay*); (*8*) *Flysh Massylian* (*Upper cretaceous*); *9*) *Tellian Calcareous marls* (*Cretaceous-Eocene*); (*10*) *Neritic limestone* (*Cenomanian-Turonian*). **b** Slope angle map. **c** Exposure map. **d** Land use type. **e** Rainfall map. **f** Distance to rivers map. **g** Distance to roads map. **h** Distance to faults

them less resistant to shear stresses and making them prone zones to gravitational movements.

In the analysis, landslide boundaries have limited only to detachment zones of active landslides (Atkinson and Massari

1998; Van den Eeckhaut et al. 2006). But, in some places where there are signs of further movement such as cracks and tilted trees, the upper portions of accumulation zones were also included.
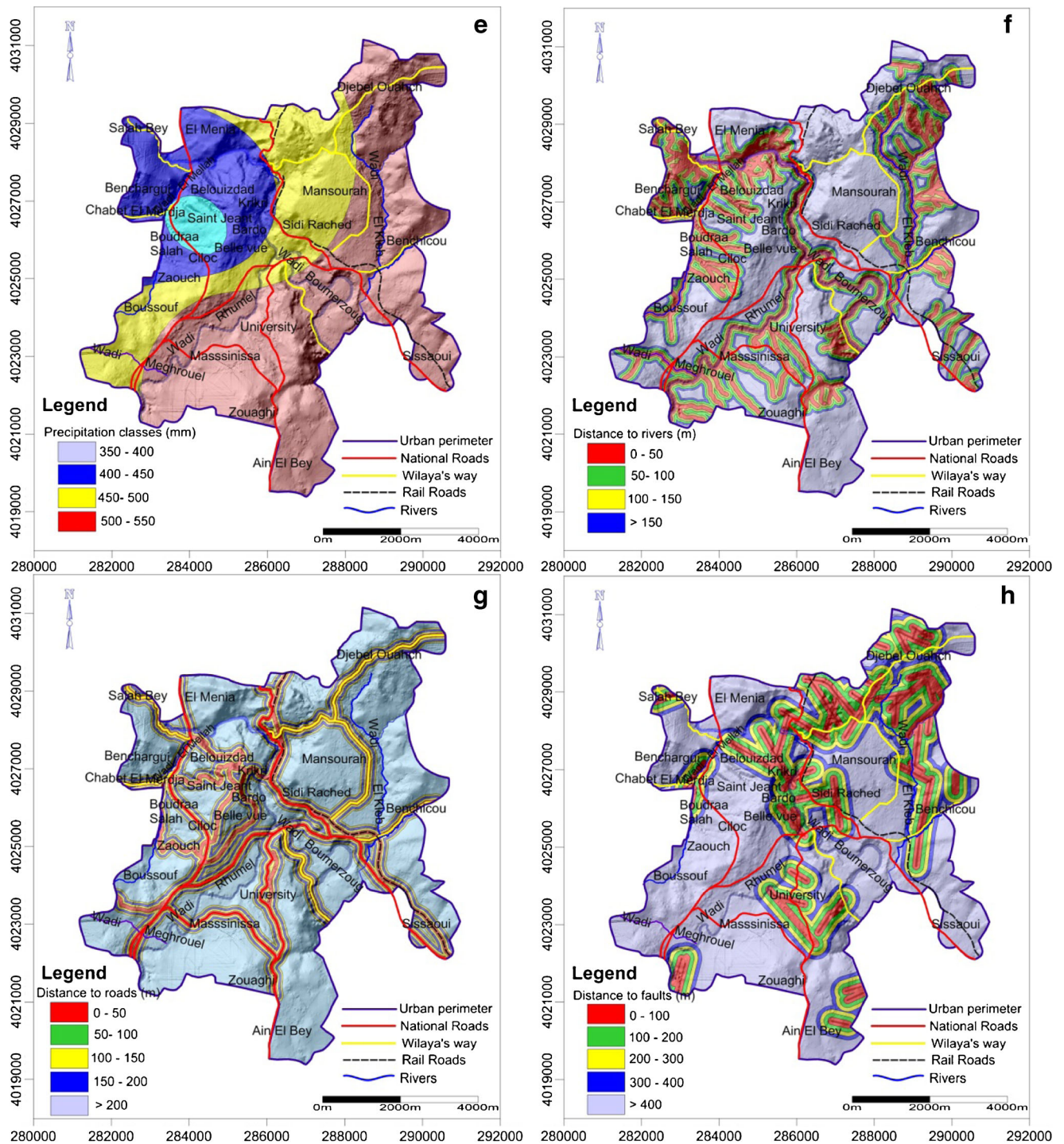
Fig. 4 (continued)

In this study, the landslide inventory is randomly divided into two independent groups, one for model training (70 %) and the other for validation (30 %) (Chung and Fabbri 2003, 2008). The landslide inventory map is helpful to understand the different triggering factors that controlling the different types of slope movement (Fig. 3).

Landslide-conditioning factors

Lithology

Lithology is one of the most important factors that influence the occurrence of landslides. Lithology with its structural and

property variations may lead to variation in strength and permeability of rocks and soils. The lithological map of the study area (Fig. 4a) defined ten (10) main lithological classes. The "Miocene marly–clay" class dominates in the study area (28 %) and has the highest landslide density (61.5 %) as shown in Table 2. While the neritic limestone class without landslide density (0).

Slope

Slope is the main causative factor because the shear forces are directly influenced by the slope gradient (Dai et al. 2001). As the slope gradient increases, it is correlated with the increased likelihood of failure. The slope gradient map of the study area was divided into five slope angle classes (Fig. 4b). The slope varies from 0 to 5° in the plain area to near vertical cliffs >45° in the steep areas. Land surfaces falling within the classes (5–15°) are strongly predominant (62 % of the total area). Landslide density is the highest in the 5–15° class, followed by the 0–5° class (Table 2). Only few landslides fall in the 15–30° class, and no landslides are observed in the 30–45° and >45° classes.

Exposure

In landslide hazard studies, exposure is considered to be an important factor influencing slope stability, since exposure related parameters, such as exposure to sunlight, drying winds, and rainfall (degree of saturation), control the concentration of the soil moisture, which in turn determinant parameter for the occurrence of landslides (Magliulo et al. 2008). The study area was classified into eight directions (Fig. 4c). Both South to West facing slopes and West to North facing slopes slightly predominate (55 % of the study are) over North to South facing slopes (26 %). The North to East facing slopes area is relatively less frequent (18 %), while only 0.2 % of the land surface is perfectly flat zone (Table 2). Therefore, in the east exposure, the landslide density is relatively low (12.5 %) and increases with the orientation angle reaching its maximum in the west exposure (43 %).

Land use

Land use is also related to the triggering and causal factors of the landslides. The woody vegetation with large and strong root systems provides both hydrological and mechanical effects that generally stabilize slopes (Gray and Leiser 1982). On the contrary, landslides occur in unvegetated or irrigated cultivated areas due to the lack of the previously mentioned effects. Five land use classes have been identified and considered in the region (Fig. 4d). Most of the study area is covered by the urban area with 37 % of the study area. The low surface is represented by forests (8 %). The correlations with landslide

density showed that the high landslide density is concentrated on the two layers (Table 2): the agriculture land (39 %) and barren land (22 %). This high landslide density can be explained by a very high activity (or high cultivated areas) of clear-cut logging as well as the increase in inappropriate new highland settlements under population growth.

Rainfall

Rainfall is widely considered as the main triggering factor of landslides hazard. Rainfall causes a change in the moisture content of the soil. Changes in moisture content increase the interstitial pore water pressure, seepage pressure, and soil weight and reduce cohesion. Precipitation database from 04 meteorological stations (Constantine, Ain El Bey, Hamma Bouziane and Fourchi) located in the vicinity of the study area has been used to create a mean annual precipitation map (Fig. 4e) by using Kriging interpolation (Isaaks and Srivastava 1989). The average seasonal precipitation from the period 1980 to 2012 ranges from 350 to 500 mm. The landslide density percentage in each rainfall class is shown in Table 2. It appears that the highest density of landslides occurs in the 400–500 mm rainfall area (45 %). This indicates clearly that landslides are directly related to precipitation.

Distance to streams

The proximity to the drainage lines is also an important controlling factor of the occurrence of landslides. Streams may negatively affect the stability by eroding the slopes or by saturating the material. Five equal buffer zones have been created within the study area in order to determine the distance to streams area affected by landslide (Fig. 4f). The correlation of the respective distance class with the landslides occurrences indicates clearly that locations close to rivers show increased landslide activity (Table 2). The analysis shows that about 30 % of landslides occur within 50 m distance to streams especially on the left bank of the Rhumel river. It is also observed that as the distance from drainage line increases, the landslide frequency decreases.

Distance to roads

Distance to roads has been considered as one of the most important anthropogenic factors influencing landslides because road-cuts are usually the source of instability (Ayalew and Yamagishi 2005). Extensive excavations, application of external loads, and vegetation removal are among the most common actions observed along the road network slopes, during their construction. These actions are also responsible for landslide triggering, that is why, the road network and buffer zones should be evaluated during the analysis. The study area has been divided into five different buffers categorized to designate the influence of the road on the slope stability (Fig. 4g).

Table 2   Frequency ratio values of the landslide-conditioning factors

Factors	Classes	% of total area (a)	% of landslide area (b)	Frequency ratio (b/a)
(A) Lithology	Neritic limestone (Cénomanian-Turonian)	3.44	0	0
	Calcareous marls of the Tellian sheet (Cretaceous-Eocene)	23.47	13.54	0.576
	Flysh Massylian Upper cretaceous	0.92	0.86	0.934
	Miocene marly clay	28.52	61.52	2.157
	Miocene conglomerates	14.21	9.79	0.688
	Quaternary lacustrine calcareous	1.28	6.03	4.710
	Pliocene lacustrine calcareous	8.35	0.49	0.058
	Quaternary recent alluvial terraces	5.31	5.61	1.056
	Quaternary ancient alluvial terraces	10.32	0.33	0.031
	Colluviums, conglomerate with muddy matrix, and thick fill quaternary	4.17	1.84	0.441
(B) Slope (°)	0–5	28.92	16.38	0.566
	5–15	62.50	70.1	1.121
	15–30	8.00	13.52	1.69
	30–45	0.48	0	0
	>45	0.08	0	0
(C) Exposure	Flat	0.2	0.3	1.5
	North	18.20	29.72	1.632
	East	25.85	12.5	0.483
	South	27.72	14.12	0.509
	West	28.01	43.36	1.548
(D) Land use	Agriculture land	12.28	39.32	3.201
	Natural forest land	8.24	8.18	0.992
	Continuous urban area	31.2	16.44	0.526
	Discontinuous urban area	37.28	10.22	0.274
	Barren land	11	21.78	1.98
	Pasture land	4.91	4.06	0.826
(E) Precipitation (mm)	350–400	2.98	0.57	0.191
	400–450	17.42	23.61	1.355
	450–500	23.4	31.18	1.332
	>500	56.2	44.64	0.794
(F) Distance to streams (m)	0–50	24.03	29.53	1.228
	50–100	17.93	24.44	1.363
	100–150	12.41	15.30	1.232
	150–200	9.24	9.16	0.991
	>200	36.39	21.57	0.592
(G) Distance to roads (m)	0–50	30.85	29.32	0.950
	50–100	20.6	21.1	1.024
	100–150	13.6	13.58	0.998
	150–200	9.35	9.7	1.037
	>200	25.6	26.3	1.027
(H) Distance to faults (m)	0–50	13.16	9.37	0.688
	50–100	12.08	9.58	0.793
	100–150	10.87	7.23	0.665
	150–200	9.46	5.91	0.624
	>200	54.43	67.91	1.247

It seems that 29 % of landslides occur within 0–150 m class, after which the frequency decreases rapidly (Table 2).

Distance to faults

Faults are zones of weakness, characterized by heavily fractured rocks which are prone to instability. Proximity (buffers) to these structures increases the probability of occurrence of landslides (Pradhan and Lee 2009). The study area has been divided into five equal area classes (Fig. 4h). The figure shows that the landslides density is higher within a distance of 200 m far from the faults (Table 2) and then the density decreases rapidly.

Landslide hazard mapping

As mentioned previously, the main purpose of the present study is to investigate and compare the landslide hazard mapping in Constantine city using five (5) models such as FR, AHP, Wf, WOE, and LR in the Constantine city, northeast of Algeria. For verification, the accuracy of results has been confirmed using the landslide inventory map.

Frequency ratio (FR) method

The FR model is one of the common methods in landslide hazard assessment. The key advantage of the FR method is the fact that it is easy to apply and the obtained results are readily intelligible. The FR method allows on to derive spatial relationship between the distribution of landslides and their conditioning factors. The FR is the ratio between the percentage of landslides in a given class and the percentage of the area in the same class. The Landslide Hazard Index (LHI) is calculated by a summation of each factor ratio value (Lee and Min 2001), as expressed in Eq. (1):

$$LHI = Fr_1 + Fr_2 + Fr_3 + \ldots\ldots + Fr_n \qquad (1)$$

Where LHI is the Landslide Hazard Index and Fr is the rating of each factor's type or range. In relationship analysis, the ratio is that of the area where landslides occurred to the total area, so that a value of 1 is an average value. If the value is >1, it means a high correlation and a value lower than 1 means a lower correlation. Therefore, the frequency ratios of each factor's type are calculated from the relationship with the landslide events as shown in Table 2.

Finally, the FR of each layer classes has been determined and a landslide hazard map (Fig. 5) has been produced prepared using the LHI map, as given in Eq. (1).

In the FR model, according to Table 2, lithological characteristics of the study area constitute an important factor in landslide occurrence. The Quaternary lacustrine calcareous
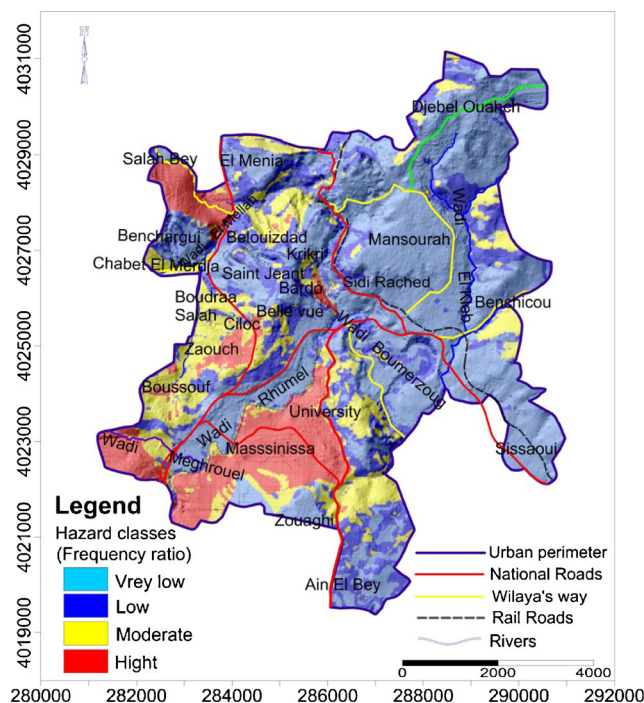

Fig. 5 Landslide hazard map obtained using the frequency ratio method

and Miocene marly clay units are found to be more susceptible and exhibited higher frequency ratio values, respectively, of 4.71 and 2.15. The slope angle is among causes of sliding because it is strongly linked to the involved forces. The (15–30°) class has the highest value of FR (1.69), while, the slope class between 0 and 15° contains the lower value of FR (0.56) indicating clearly that the FR increases proportionally with the slope angle. Slope exposure analyses shows that most of the landslides occurred at the north (1.63), west (1.54), and flat (1.5) directions. The variation in the vegetation in a given area is a parameter that affects seriously the slope failures, and the landslide hazard decreases with the presence of vegetation. This is confirmed in this study, where the land use analysis showed that the landslide commonly occurred in the uncultivated agriculture (3.20) and barren areas (1.98). For the closer distances to the rivers, FR values greater than one (1) have been obtained indicating a high probability of landslide occurrence. The distances between 100 and 150 and 150–200 m have higher values of FR, respectively, 1.36 and 1.23, indicating a high probability of landslide occurrence. The distance to road is usually taken into account in landslide hazard assessments. The proximity to roads gives, respectively, values 0.95 and 1.02 for distances between 0 to 50 and 50 to 100 m. Also, the obtained results show that as the distance from faults increases, the landslide frequency increases (Table 2). The intervals 150–200 and >200 m show a FR values of, respectively, 0.62 and 1.24. FR analysis shows that higher FR values were distributed in higher precipitation zones (Table 2) with 1.33 observed in (450–500 mm) class and 1.35 (400–450 mm)

class. This means that the landslide probability increases with the amount of precipitation.

Weighting factor (W_f) method

The weighting factor (W_f) method (Cevik and Topal 2003) known also as the InfoVal method used in this study is a modification of the statistical index (Wi) method, namely, the bivariate statistical method (Van Westen 1997). It is outlined and considered in many works as a simple and quantitatively suitable method in landslide hazard mapping.

The statistical index (Wi) method is based on a statistical correlation of the predisposing factors and the distribution of landslide areas. For each predisposing factor, the density of the landslide of the training set in each class is evaluated. The weight value for each class is defined as the natural logarithm of the landslide density in the categorical unit divided by the landslide density in the entire map:

$$Wi = In \frac{\text{Densclass}}{\text{Densmap}} = In\left(\frac{Npix(Si)/Npix(Ni)}{SNpix(Si)/SNpix(Ni)} \right) \qquad (2)$$

Where Wi is the weight given to the class of a particular thematic layer, *Densclass* is the landslide density within the thematic class, *Densmap* is the landslide density within the entire thematic layer, *Npix* (*Si*) is the number of landslide pixels in a certain thematic class, *Npix* (*Ni*) is the total number of pixels in a certain thematic class, and *n* is the number of classes in the thematic map. *SNpix* (*Ni*) is the number of pixels of all landslide, and *SNpix* (*Ni*) is the total number of all pixels. The natural logarithm is used to accommodate the large variation in the weights.

However, the statistical index method considers that each parameter/thematic map has an equal effect on landslides, which may not be the case in reality (Oztekin and Topal 2005). Therefore, a weighting factor (W_f) for each parameter map has been evaluated. For this purpose, first, the Wi value of each pixel has been determined by the statistical index method, then, all pixel values belonging to each layer are summed. By using the maximum and minimum of all layers, the results are stretched (Cevik and Topal 2003). Finally, the weighting factor ranging from 1 to 100 for each layer is determined by the following equation:

$$W_f = \frac{(\text{TWi}_{value}) - (\text{MinTWi}_{value})}{(\text{MaxTWi}_{value}) - (\text{MinTWi}_{value})} *100 \qquad (3)$$

Where W_f is the weighting factor calculated for each layer, TWi$_{value}$ is the total weighting index value of cells within the landslide bodies for each layer, MinTWi$_{value}$ is the minimum total weighting index value within the selected layers, and Max TWi$_{value}$ is the maximum total weighting index value within the selected layers.

By using the Eq. (3), the weighting factor (W_f) values of each layer have been determined and reported in Table 3. For the analyses, the W_f value for each layer has been multiplied by the Wi value of each attribute, and finally, all causal factor maps have been summed in order to generate the final landslide hazard map (Fig. 6) from the Infoval or weighting factor. The resulted map has been reclassified by dividing the total number of elements (W_f value), mainly, into five distinct classes using the standard deviation method: low (−23 to −0.89), moderate (−0.89 to 1.03), high (1.03 to 2.40), and very high hazard (2.40 to 5.85). To control the accuracy of the landslide hazard maps produced by W_f method, the landslide inventory map and hazard map have been statistically compared.

Logistic regression (LR) method

The logistic regression (LR) is one of the most common statistical approach used in geosciences especially in landslide assessment. Logistic multiple regression allows one to evaluate a multivariate regression relationship between a dependent (landslides) and independent variables (such as slope angle, exposure, and lithology). As stated by Lee and Sambath (2006), logistic regression is useful for predicting the presence or absence of a characteristic or outcome based on value of a set of predictor variables. The important advantages of LR is that, through addition of an appropriate link function to the usual linear regression model, the variables may be either continuous or discrete, or any combination of both types, and they do not necessarily have normal distributions (Lee and Sambath 2006; Lee and Pradhan 2007). In the present study, the dependent variable is a binary variable representing the presence (1) or the absence (0) of a landslide, while the independent variables can be continuous, discrete, dichotomous, or a mix of any of these.

The algorithm of logistic regression applies maximum likelihood estimation after transforming the dependent variable into a logic variable representing the natural logarithm of the odds of the dependent occurring or not (Atkinson and Massari 1998; Bai et al. 2010). The mentioned model can be expressed according to following equation (Lee and Pradhan 2007):

$$P = \left(\frac{1}{1 + e^{-z}} \right) \qquad (4)$$

Where P is the estimated probability of landslide occurrence, varying from 0 to 1 on an S-shaped curve, and Z is the a linear combination defined as by the following Equation (Eq. 5) and its value varies from −∞ to +∞:

$$Z = \text{intercept} + b_1 x_1 + b_2 x_2 + b_3 x_3 + \dots + b_n X_n \qquad (5)$$

Where here, b_1, b_2, b_3, and b_n are the slope coefficients of the logistic regression model and x_1, x_2, x_3, and x_n are the independent variables.

Table 3 Weighting values (Wi) calculated, for each class of the selected landslide causal factors

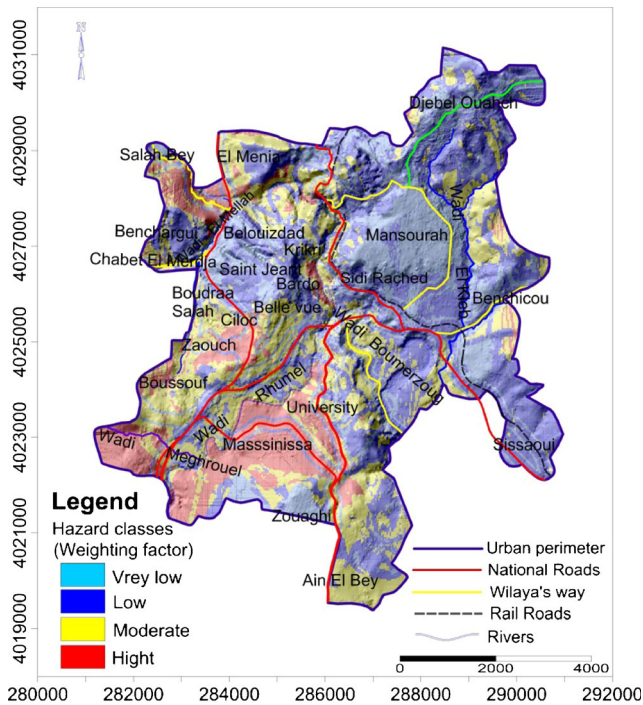| Factors	Classes	Pixels in classes	Landslide pixels in classes	Statistical index (Wi)	Wf in classes	Weighting factor (Wf)
(A) Lithology	Neritic limestone (Cénomanian-Turonian)	2322	0	0	0	100
	Calcareous marls of the Tellian sheet (Cretaceous-Eocene)	15863	1155	−0.559	−55.9	
	Flysh Massylian upper cretaceous	619	73	−0.066	−6.6	
	Miocene marly clay	19271	5244	0.769	76.9	
	Miocene conglomerates	9608	834	−0.372	−37.2	
	Quaternary lacustrine calcareous	869	515	1.548	154.8	
	Pliocene lacustrine calcareous	5650	42	−2.830	−283	
	Quaternary recent alluvial terraces	3587	478	0.056	5.6	
	Quaternary ancient alluvial terraces	6976	29	0.032	3.2	
	Colluviums, conglomerate with muddy matrix, and thick fill quaternary	2825	156	−0.824	−82.4	
(B) Slope (°)	0–5	19554	1397	−0.567	−56.15	99.03
	5–15	42245	5976	0.115	11.38	
	15–30	5408	1153	0.525	52	
	30–45	327	0	0	0	
	>45	56	0	0	0	
(C) Exposure	Flat	136	27	0.454	33.59	74.63
	North	12307	2534	0.491	36.56	
	East	17475	1065	−0.726	−53.72	
	South	18739	1203	−0.674	−54.18	
	West	18933	3697	0.438	32.09	
(D) Land use	Agriculture land	7633	3352	1.248	122.18	98.54
	Natural forest land	4904	698	0.121	11.82	
	Continuous urban area	20419	1401	−0.607	−59.81	
	Discontinuous urban area	24528	872	−1.265	−124.16	
	Barren land	6786	1856	0.775	76.36	
	Pasture land	3320	347	−0.186	−18.32	
(E) Precipitation (mm)	350–400	2019	49	−1.647	−164.7	100
	400–450	11771	2013	0.305	30.5	
	450–500	15817	2658	0.287	28.7	
	>550	37983	3806	−0.229	−22.9	
(F) Distance to streams (m)	0–50	16236	2517	0.207	20.41	98.64
	50–100	12116	2084	0.311	30.67	
	100–150	8383	1305	0.211	20.81	
	150–200	6253	781	−0.008	−0.78	
	>200	24602	1839	−0.522	−51.49	
(G) Distance to roads (m)	0–50	20848	2499	−0.049	−4.19	85.55
	50–100	13927	1799	0.024	1.71	
	100–150	9191	1158	−5.699	−487.54	
	150–200	6323	827	0.037	3.16	
	>200	17301	2243	0.028	2.39	
(H) Distance to faults (m)	0–50	8894	800	−0.337	−28.99	87.61
	50–100	8163	816	−0.231	−20.15	
	100–150	7344	617	−2.476	−216.39	
	150–200	6395	504	−0.469	−40.3	
	>200	36794	5789	0.222	19.44	

Fig. 6 Landslide hazard map obtained using the weighting factor method

Using the logistic regression model, the spatial relationship between landslide occurrence and landslide affecting factors is assessed. For this purpose, the spatial databases of all the conditioning factors and landslides have been converted into grid format and, then, into Excel data format files to be used in the statistical package XLSTAT 2014 trial version. Then, the correlation between landslide event and landslide affecting factors has been estimated, and the logistic regression model has been run to obtain the coefficients of the landslide-conditioning factors. The Hosmer and Lemeshow test showed that the goodness of fit of the equation can be accepted because the significance of chi-square is larger than 0.05 (0.09). A higher R-square value of Cox and Snell R^2 (0.892) and Nagelkerke R^2 (1.365) indicates a better model. The relative operating characteristic (ROC) value of 0.9502 indicates a good correlation between the independent and dependent variables.

The weighting of the factor classes is based on the percentage area of landslides in the homogenous units. The percentage area of landslides which depend on each factor has been identified by calculating the ratio of the observed landslide area to the area of homogeneous units. The weight factor for each class of a specific factor has been calculated by summing the ratios for each class in different units. Weight factors have been transferred to the quantitative values from 0 to 10. The class with the maximum of the summation percentage area has been given a weight of 10, and the in other classes, the given weight is <10 based on their proportions.

The weight factor and the logistic regression coefficient for each thematic layer are shown in Table 4. Finally, the binary logistic regression model developed for the study area is given in Eq. 6:

$$
\begin{aligned}
Z = {} & -1{,}099 + 1.99{*}lithology(1) + 2.184{*}lithology(2) + 1.256{*}lithology(3) + 2.048{*} \\
& lithology(4) + 2.105{*}lithology(5) - 0.008{*}lithology(5) + 2.112{*}lithology(6) - 0{,}005{*} \\
& lithology(8) - 0{,}028{*}lithology(9) - 0.007{*}Slope(1) + 1.552{*}Slope(2) + 1.926{*}Slope(3) + \\
& 1.890{*}Slope(4) + 1.255{*}Slope(5) - 0.220{*}Exposure(1) + 1.256{*}Exposure(2) + 2.016{*} \\
& Exposure(3) + 1.255{*}landuse(1) + 2.001{*}landuse(2) + 1.803{*}landuse(3) + 1.952{*}landuse \\
& (4) + 1.675{*}landuse(5) + 2.100{*}landuse(6) - 0.012{*}Precipitation(1) + 1.699{*}Precipitation \\
& (2) + 1.540{*}Precipitation(3) + 1.255{*}Precipitation(4) + 1.255{*}River(1) + 1.417{*}River(2) + \\
& 1.709{*}River(3) + 2.197{*}River(4) + 1.6707{*}River(5) + 2.197{*}Road(1) + 1.5195{*}Road(2) \\
& + 1.761{*}Road(3) + 1.120{*}Road(4) + 2.064{*}Fault(1) + 2.097{*}Fault(2) - 0.082{*}Fault(3) + \\
& 2.010{*}Fault(4)
\end{aligned}
$$

(6)

According to Table 4 and Eq. 6, land use, precipitation, distance to streams, and distance to roads are positively related to the occurrence of landslides because of their positive coefficients. On the other hand, slope degree has a positive role in landslides occurrence except for the (0–5°) class which has a negative effect with a values of −0.007. In the case of the slope exposure, south (0), north (1.25), east (2.01), and west (0) facings have positive coefficients. Unlikely, flat facing has a value of −0.22. For the precipitation factor, results showed that only rainfall classes ranging from 350 to 400 did not have any role in landslides occurrence with a coefficient value of 0.875, while the remaining classes are positively related to the probability of landslides formation. Based on the results of the logistic regression for the lithology factor, it appears that the lithological formations of groups 7, 9, and 10 (Table 4) have an inverse effect on landslide hazard with a negative values of −0.008, −0.005, and −0.028, respectively, while the remaining classes have a positive relation with the landslide occurrence showing positive value has been observed.

The probability of landslide occurrence has been calculated by using the above logistic regression

Table 4　Logistic regression coefficients for each class of the selected landslide causal factors

| Factors	Classes	% of total area	% of landslide area	Factor weight (W)	Logistic regression coefficients
(A) Lithology					
Lithology (1)	Neritic limestone (Cénomanian-Turonian)	3.44	0	0.00	0.000
Lithology (2)	Calcareous marls of the Tellian sheet (Cretaceous-Eocene)	23.47	13.54	2.20	1.990
Lithology (3)	Flysh Massylian upper cretaceous	0.92	0.86	0.14	2.184
Lithology (4)	Miocene marly clay	28.52	61.52	10.00	1.256
Lithology (5)	Miocene conglomerates	14.21	9.79	1.59	2.048
Lithology (6)	Quaternary lacustrine calcareous	1.28	6.03	0.98	2.105
Lithology (7)	Pliocene lacustrine calcareous	8.35	0.49	0.08	−0.008
Lithology (8)	Quaternary recent alluvial terraces	5.31	5.61	0.91	2.112
Lithology (9)	Quaternary ancient alluvial terraces	10.32	0.33	0.05	−0.005
Lithology (10)	Colluviums, conglomerate with muddy matrix, and thick fill quaternary	4.17	1.84	0.30	−0.028
(B) Slope (°)					
Slope (1)	0–5	28.92	16.38	2.34	−0.007
Slope (2)	5–15	62.50	70.1	10.00	1.552
Slope (3)	15–30	8.00	13.52	1.93	1.926
Slope (4)	30–45	0.48	0	0.00	1.890
Slope (5)	>45	0.08	0	0.00	1.256
(C) Exposure					
Aspect (1)	Flat	0.2	0.3	0.07	−0.220
Aspect (2)	North	18.20	29.72	6.85	1.256
Aspect (3)	East	25.85	12.5	2.88	2.016
Aspect (4)	South	27.72	14.12	3.26	0.000
Aspect (5)	West	28.01	43.36	10.00	0.000
(D) Land use					
Land use (1)	Agriculture land	12.28	39.32	10.00	1.256
Land use (2)	Natural forest land	8.24	8.18	2.08	2.001
Land use (3)	Continuous urban area	31.2	16.44	4.18	1.804
Land use (4)	Discontinuous urban area	37.28	10.22	2.60	1.953
Land use (5)	Barren land	11	21.78	5.54	1.676
Land use (6)	Pasture land	4.91	4.06	1.03	2.100
(E) Precipitation (mm)					
Precipitation (1)	350–400	2.98	0.57	0.13	−0.012
Precipitation (2)	400–450	17.42	23.61	5.29	1.699
Precipitation (3)	450–500	23.4	31.18	6.98	1.540
Precipitation (4)	>550	56.2	44.64	10.00	1.256
(F) Distance to streams (m)					
Distance to streams (1)	0–50	24.03	29.53	10.00	1.256
Distance to streams (2)	50–100	17.93	24.44	8.28	1.418
Distance to streams (3)	100–150	12.41	15.30	5.18	1.710
Distance to streams (4)	150–200	9.24	9.16	3.10	2.197
Distance to streams (5)	>200	36.39	21.57	7.30	1.671
(G) Distance to roads (m)					
Distance to roads (1)	0–50	30.85	29.32	10.00	2.197
Distance to roads (2)	50–100	20.6	21.1	7.20	1.520
Distance to roads (3)	100–150	13.6	13.58	4.63	1.761
Distance to roads (4)	150–200	9.35	9.7	3.31	2.197
Distance to roads (5)	>200	25.6	26.3	8.97	1.120
(H) Distance to faults (m)					
Distance to faults (1)	0–50	13.16	9.37	1.38	2.065
Distance to faults (2)	50–100	12.08	9.58	1.41	2.097
Distance to faults (3)	100–150	10.87	7.23	1.06	−0.082
Distance to faults (4)	150–200	9.46	5.91	0.87	1.065
Distance to faults (5)	>200	54.43	67.91	10.00	2.010
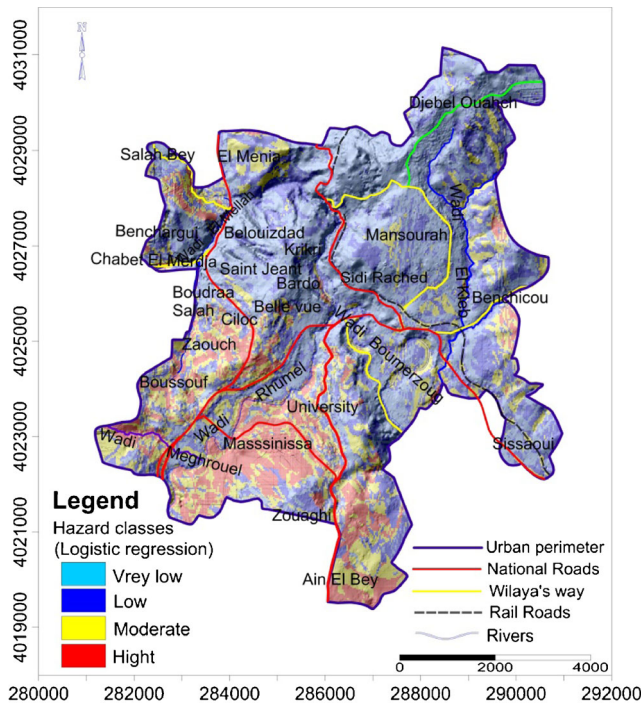
Fig. 7 Landslide hazard map obtained using the logistic regression method

coefficients. The probability ranges from 0.94 to 1. The obtained landslide hazard map has been obtained based on the logistic regression model (Fig. 7). The probability map has been divided into four hazard classes: very low (0.9444–0.9991), low (0.9991–0.9996), moderate (0.9996–0.9998), and high (0.9998–1).

Analytical hierarchy process

The analytical hierarchy process (AHP) is a theory of measurement dealing with quantifiable and intangible criteria applied to numerous cases, such as decision theory and conflict resolution (Vargas 1990). This technique has been already used for landslide hazard mapping and

widely applied, and the results showed encouraging (Ayalew et al. 2005; Yalcin et al. 2011). The popularity of the AHP is due to its simplicity, flexibility, ease of use, and interpretation. The AHP is a multi-objective, multi-criteria decision-making approach, enables to organize, analyze, and solve complex decision problems (Saaty 1980). It is based on three major main steps: decomposition, comparative judgment, and synthesis of priorities. The decomposition principle is applied to structure complex problems into component factors and hierarchies them. The comparative judgment principle of AHP requires pair-wise comparison of the decomposed elements within a given level of hierarchal structure with respect to the next higher level. The synthesis principle of AHP takes each of the derived ratio local scale priorities in the various levels of the hierarchy and constructs a composite set of priorities for the elements at the bottom of the hierarchy. The AHP provides a numerical fundamental scale, ranging from 1 to 9 to calibrate the quantitative and qualitative performances of the priorities (Table 5) (Saaty 2008). This matrix ultimately enters in expert choice (EC) software and calculates the final weight for each conditioning factor with a consistency ratio (CR) expressed as:

$$CR = (CI/RI) \tag{7}$$

Where RI is the average of the resulting consistency index depending on the order of the matrix given by Saaty (1980) and CI is the consistency index expressed as:

$$CI = (\lambda_{max} - n)/(n-1) \tag{8}$$

Where λ_{max} is the largest or principal eigenvalue of the matrix and can be easily calculated from the matrix, and n is the order of the matrix. If CR is less than 10 %, then the matrix can be considered as having an acceptable consistency (Saaty 1977). A CR greater than 10 % requires revision of the judgment in the matrix

Table 5 Fundamental scale for pair-wise comparisons (Saaty 2000)

Intensity of importance	Definition	Explanation
1	Equal importance	Two activities contribute equally to the objective
3	Moderate importance	Experience and judgment strongly favor one activity over another
5	Strong importance	The evidence favoring one activity over another is of the highest possible order of affirmation
7	Very strong or demonstrated importance	An activity is favored very strongly over another, its dominance demonstrated in practice
9	Extreme importance	The evidence favoring one activity over another is of the highest possible order of affirmation
2,4,6,8	Intermediate values between adjacent scale values	When compromise is needed
Reciprocals	Opposites	Used for inverse comparison

Table 6   Preferences and weights of conditioning factors by analytical hierarchy

Conditioning factors	(1)	(2)	(3)	(4)	(5)	(6)	(7)	(8)	Weight (W)	Weight (%)
(1) Lithology	1	2	2	3	2	2	3	5	0.228	22.80
(2) Precipitation	1/2	1	3	4	3	3	3	5	0.231	23.14
(3) Slope	1/2	1/3	1	3	3	3	3	4	0.166	16.63
(4) Land use	1/3	1/4	1/3	1	2	2	2	3	0.09	09.00
(5) Distance to streams	1/2	1/3	1/3	0.5	1	2	3	4	0.102	10.20
(6) Exposure	1/2	1/3	1/3	0.5	0.5	1	3	4	0.088	08.80
(7) Distance to roads	1/3	1/3	1/3	0.5	0.33	0.33	1	4	0.061	06.16
(8) Distance to faults	1/4	1/5	1/4	0.33	0.25	0.25	0.25	1	0.030	03.00

λmax = 08.08; CI = 0.0114 = 1.14; consistency ratio CR = 0.008

due to an inconsistent treatment of particular rating factor. Finally, the landslide hazard map using AHP model has been constructed by using the following equation:

$$LHI_{AHP} = Lithology \times W_{AHP} + land\ use \times W_{AHP}$$
$$+ Slope\ degree \times W_{AHP}$$
$$+ slope\ Exposure\ x\ W_{AHP}$$
$$+ distance\ from\ rivers \times W_{AHP}$$
$$+ distance\ from\ roads \times W_{AHP}$$
$$+ Distance\ to\ faults \times W_{AHP} + Altitude$$
$$\times W_{AHP} + Precipitation \times W_{AHP} \qquad (9)$$

Where, W_{AHP} is the weightage for each landslide-conditioning factor.

Using AHP method, the levels and weight values of the conditioning factors have been defined and calculated (Table 6). According to the degree of importance, land use, lithology, and slope appear as the most important factors that influence landslide occurrence with, respectively, values of 0.231, 0.228, and 0.166, whereas distance to fault is the less influencing landslide occurrence with a value of 0.03 (Table 6). The following values: λmax=08.08, CI=0.011 (1.14 %) and CR=0.008, means that the pair-wise matrix is consistent (threshold CR<0.10) and can be used for assigning the weight criteria. Using the above factors evaluation and its weights, the equation for landslide hazard is given as below:

$$LHI_{AHP} = 0.228 \times Lithology + 0.231 \times Precipitation$$
$$+ 0.166 \times Slope + 0.09 \times Land\ use$$
$$+ 0.102 \times Distance\ to\ streams$$
$$\times +0.088 \times Exposure + 0.061$$
$$\times Distance\ from\ roads + 0.030$$
$$\times Distance\ to\ faults. \qquad (10)$$

The weight values of the different factor classes have been determined based on the percentages of the area of each class covered by the landslide area (Table 7). In the presence of lithology, the higher percentage of the area of Miocene marly clay factor class covered by the landslide, thus it was given highest factor class weight value, i.e., 100, which when multiplied with the factor weight gave the actual weight value of 22.8 as shown in Table 7. The lowest percentage of area of Neritic limestone factor class covered by the landslide was given the lowest factor class weight value of 0, when multiplied with the factor weight yield gave the value of 0. Similarly, the weight values of different factor classes have been determined and seen in Table 7.

As a result of the AHP analyses, a landslide hazard map has been established for the urban area of Constantine city (Fig. 8) by summation of all weighted layers as given in Eq. (10). The resulting landslide hazard map presents four hazard classes following the LHI value: 33.5 % (2.921<LHI>6.831) of the area falls in very low hazard class, 27.3 % (6.831<LHI>8.407) in low hazard class, 20 % (8.407<LHI>11.307) in medium hazard class, while very small portion 19.3 % (11.307<LHI>16.4) of the area falls in the high hazard class.

Weights of evidence method

The weights of evidence (WOE) is a statistical method that uses the log linear form of the Bayesian probability model to estimate the relative importance of evidence by statistical means. This method was first applied to the identification of mineral potential (Bonham-Carter et al. 1989) and then to landslide susceptibility and hazard mapping (Van Westen 1993; Van Westen et al. 2003; Suzen and Doyuran 2004).

This method calculates the weight for each landslide predictive factor (B) based on the presence or absence of landslides (L) within the area as follows (Bonham-Carter 1994):

$$W^+ = In \frac{p(B/L)}{P\left(B/\overline{L}\right)} \qquad (11)$$

$$W^- = In \frac{p\left(\overline{B}/L\right)}{P\left(\overline{B}/\overline{L}\right)} \quad (12)$$

Where P is the probability of ratio and ln is the natural logarithm (logit), in order to estimate the conditional probability of landslide occurrence. B is the presence of the predictive factor, and L is the presence of landslide. The overbar sign "$^-$" represents the absence of the class and/or landslide. Positive W^+ and negative W^- weights are indications of the positive and

negative correlations between the landslides occurrence and the presence of the predictable variable, respectively.

The difference between the positive and negative weights, as computed for each class of each parameter analyzed, is known as the weight contrast WC:

$$WC = W^+ - W^- \quad (13)$$

The magnitude of the contrast reflects the overall spatial association between the predictable variable and landslides.

Table 7 Weight values of factor classes by analytical hierarchy process

| Factors	Classes	% of total area	% of landslide area	Weight by % of landslide area	Factor weight (W)	Actual factor weight (W)
(A) Lithology	Neritic limestone (Cénomanian-Turonian)	3.44	0	0	0.228	0
	Calcareous marls of the Tellian sheet (Cretaceous-Eocene)	23.47	13.54	22.009	0.228	5.018
	Flysh Massylian upper cretaceous	0.92	0.86	1.39	0.228	0.318
	Miocene marly clay	28.52	61.52	100	0.228	22.80
	Miocene conglomerates	14.21	9.79	15.91	0.228	3.62
	Quaternary lacustrine calcareous	1.28	6.03	9.80	0.228	2.23
	Pliocene lacustrine calcareous	8.35	0.49	0.79	0.228	0.18
	Quaternary recent alluvial terraces	5.31	5.61	9.11	0.228	2.07
	Quaternary ancient alluvial terraces	10.32	0.33	0.53	0.228	0.12
	Colluviums, conglomerate with muddy matrix, and thick fill quaternary	4.17	1.84	3	0.228	0.68
(B) Slope (°)	0–5	28.92	16.38	23.36	0.166	3.87
	5–15	62.50	70.1	100	0.166	16.63
	15–30	8.00	13.52	19.28	0.166	3.20
	30–45	0.48	0	0	0.166	0
	>45	0.08	0	0	0.166	0
(C) Exposure	Flat	0.2	0.3	0.69	0.09	0.06
	North	18.20	29.72	68.54	0.09	6.16
	East	25.85	12.5	28.82	0.09	2.59
	South	27.72	14.12	32.56	0.09	2.93
	West	28.01	43.36	100	0.09	9.00
(D) Land use	Agriculture land	12.28	39.32	100	0.231	23.14
	Natural forest land	8.24	8.18	20.8	0.231	4.80
	Continuous urban area	31.2	16.44	41.81	0.231	9.65
	Discontinuous urban area	37.28	10.22	26	0.231	6.00
	Barren land	11	21.78	55.39	0.231	12.79
	Pasture land	4.91	4.06	10.32	0.231	2.38
(E) Precipitation (mm)	350–400	2.98	0.57	1.27	0.088	0.11
	400–450	17.42	23.61	52.88	0.088	4.65
	450–500	23.4	31.18	69.84	0.088	6.14
	>550	56.2	44.64	100	0.088	8.80
(F) Distance to streams (m)	0–50	24.03	29.53	100	0.102	10.20
	50–100	17.93	24.44	82.76	0.102	8.44
	100–150	12.41	15.30	51.81	0.102	5.28
	150–200	9.24	9.16	31.01	0.102	3.16
	>200	36.39	21.57	73.04	0.102	7.45
(G) Distance to roads (m)	0–50	30.85	29.32	100	0.061	6.16
	50–100	20.6	21.1	71.96	0.061	4.38
	100–150	13.6	13.58	46.31	0.061	2.82
	150–200	9.35	9.7	33.08	0.061	2.01
	>200	25.6	26.3	89.69	0.061	5.47
(H) Distance to faults (m)	0–50	13.16	9.37	13.79	0.030	0.41
	50–100	12.08	9.58	14.10	0.030	0.42
	100–150	10.87	7.23	10.64	0.030	0.31
	150–200	9.46	5.91	8.71	0.030	0.26
	>200	54.43	67.91	100	0.030	3.00
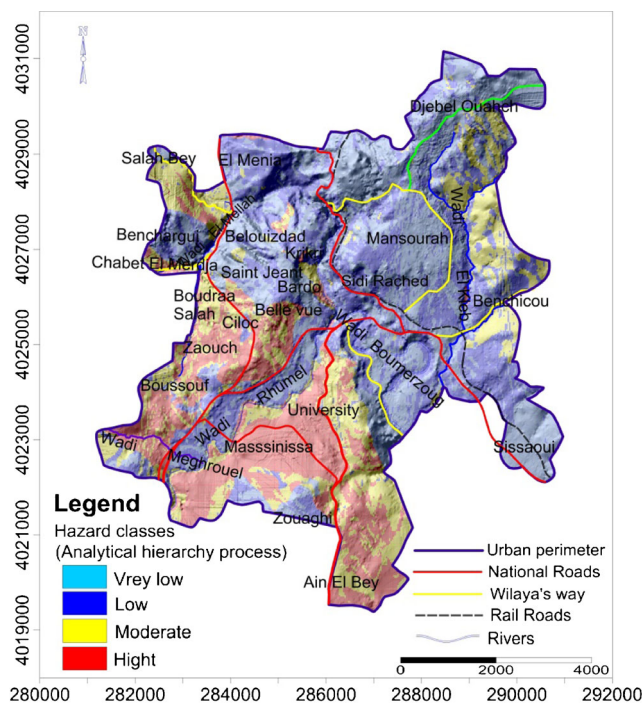
Fig. 8 Landslide hazard map obtained using the analytical hierarchy process method

The value of WC is typically between 0 and 2; when the value of C tends to zero, the presence of the considered parameter does not affect the distribution of landslides in the area; whereas, when C is approximately two or more, the correlation is significant (Barbieri and Cambuli 2009).

In this study, firstly, the various thematic maps showing the landslides affecting factors have been overlapped with the landslide map. On the basis of these intersections, for each of the landslide-related factors, the weights, contrasts, and weights of evidence probability values have been calculated using Eqs. 11, 12, and 13 (Table 8). Then, the conditional independence has been tested before the integration of the patterns predictor to map the landslide hazard. The chi-square values to test the conditional independence between all pairs of binary patterns for each factor have been calculated at the 95 % significance level and 1° of freedom. The calculated chi-square values are greater than values of the table (7.9) suggest that the pairs are not significantly different.

The resulting contrast, as shown in Table 8, indicates directly the importance of each factor for the landslides occurrence. The contrast is positive for favorable factors to the occurrence and negative for unfavorable factors to the occurrence of landslides. Results of contrast value (Table 8) analysis showed that factors with highest landslide probabilities correspond to Miocene marly clay and Quaternary Colluviums formations, the agriculture land, the (450–500 mm) of precipitation, (5–15°) of slope, the flat of slope exposure, the (100–150 m) of distance to river classes. It can also be concluded from Table 8 that the contrasts of the factors indicate that there

is no relation with the occurrence of landslides, as evidenced by the weights close to 0. For instance, distance from road classes show values near zero, indicates that the distance from roads is not a very sensitive predicting factor in the study area.

Weights are assigned respectively to the classes of each thematic layer, to produce weighted thematic maps, which have been overlaid and numerically added according to Eq. (14) in order to produce a Landslide Hazard Index (LHI) map:

$$
\begin{aligned}
\text{LHI}_{WC} = {} & \text{WC Slope} + \text{WC Exposure} + \text{WC Fault} \\
& + \text{WC River} + \text{WC Precip} \\
& + \text{WC Landuse} + \text{WC Road} \\
& + \text{WC Lithology}
\end{aligned}
\tag{14}
$$

where WC Slope, WC Exposure, WC Fault, WC River, WC Precip, WC Land use, WC Road, and WC Lithology are distribution-derived weights relative to slope, exposure, fault, distance to river, precipitation, land use, distance to road, and lithology maps, respectively.

Thus, the landslide hazard map (Fig. 9) of Constantine city is prepared from the respective LHI values. The range of landslide hazard is classified into four categories: very low (−8.58–−1.8), low (−1.8–0.7), moderate (0.7–3.15), and high (3.15–9.55).

In this study, the LHMs have been divided into four classes based on the standard deviations method, since the data obtained values in the LHMs by using the FR, Wf, LR, WOE, and AHP models show a normal distribution (Suzen and Doyuran 2004; Ayalew et al. 2005; Yalcin et al. 2011).

Validation and comparison of landslide hazard maps

The most important task, in landslide hazard modeling, is to perform the validation of the predicted results. Without validation, the predicted models and prepared maps are less useful and without scientific significance (Chung and Fabbri 2003). There are different ways to validate LHM using mathematical and statistical tools. The most useful methods to represent the quality and the performance of LHM used in the literature are the receiver operating characteristics (ROC) and the statistics rules for spatial effective LHMs. The validation process has been performed by comparing the known landslide location data with the LHMs. In this comparison, the landslide activity map is matched with the LHMs. Then, the distribution of current landslide area is determined according to the landslide hazard classes in order to test if the percentage of landslides is effectively increasing with the hazard degree.

Table 8 Weighting values (WC) calculated, for each class of the selected landslide causal factors

Factors	Classes	Pixels in classes	Landslide pixels in classes	Weights (+)	Weights (−)	Weight contrast (WC)
(A) Lithology	Neritic limestone (Cénomanian-Turonian)	2322	0	0	0	0
	Calcareous marls of the Tellian sheet (Cretaceous-Eocene)	15863	1155	−0.61	0.19	−0.8
	Flysh Massylian upper cretaceous	619	73	0.11	0.001	0.10
	Miocene marly clay	19271	5244	0.97	−0.69	1.66
	Miocene conglomerates	9608	834	−0.44	0.05	−0.49
	Quaternary lacustrine calcareous	869	515	2.48	−0.06	2.54
	Pliocene lacustrine calcareous	5650	42	−3.11	0.09	−3.2
	Quaternary recent alluvial terraces	3587	478	0.07	−0.004	0.074
	Quaternary ancient alluvial terraces	6976	29	−3.60	0.11	−3.71
	Colluviums, conglomerate with muddy matrix, and thick fill quaternary	2825	156	2.72	0.03	2.69
(B) Slope (°)	0–5	19554	1397	−0.62	0.18	−0.8
	5–15	42245	5976	0.13	−2.25	2.38
	15–30	5408	1153	0.61	−0.06	0.67
	30–45	327	0	0	0	0
	>45	56	0	0	0	0
(C) Exposure	Flat	136	27	1.09	0	1.09
	North	12307	2534	0.59	0.32	0.27
	East	17475	1065	−0.81	−1.4	0.59
	South	18739	1203	−0.72	0.29	−1.01
	West	18933	3697	0.54	−0.27	0.81
(D) Land use	Agriculture land	7633	3352	1.71	−0.49	2.2
	Natural forest land	4904	698	0.13	−0.49	0.62
	Continuous urban area	20419	1401	−0.69	−0.31	−0.38
	Discontinuous urban area	24528	872	−1.38	−0.03	−1.35
	Barren land	6786	1856	0.96	−0.79	1.75
	Pasture land	3320	347	−0.22	−0.42	0.2
(E) Precipitation (mm)	350–400	2019	49	−1.79	−0.19	−1.6
	400–450	11771	2013	0.36	−0.08	0.44
	450–500	15817	2658	0.34	−0.12	0.46
	>550	37983	3806	−0.25	0.27	−0.52
(F) Distance to streams (m)	0–50	16236	2517	0.23	−0.26	0.49
	50–100	12116	2084	−1.58	−0.26	−1.32
	100–150	8383	1305	0.31	−0.16	0.47
	150–200	6253	781	−0.02	−0.09	0.07
	>200	24602	1839	−0.59	0.24	−0.83
(G) Distance to roads (m)	0–50	20848	2499	−0.06	0.02	−0.08
	50–100	13927	1799	0.04	−0.01	0.05
	100–150	9191	1158	−0.007	0.001	−0.008
	150–200	6323	827	−0.03	−0.003	−0.027
	>200	17301	2243	0.03	−0.17	0.2
(H) Distance to faults (m)	0–50	8894	800	−0.49	0.09	−0.58
	50–100	8163	816	−0.28	0.09	−0.37
	100–150	7344	617	−0.45	0.10	−0.55
	150–200	6395	504	−0.58	0.10	−0.68
	>200	36794	5789	0.25	−0.39	0.64
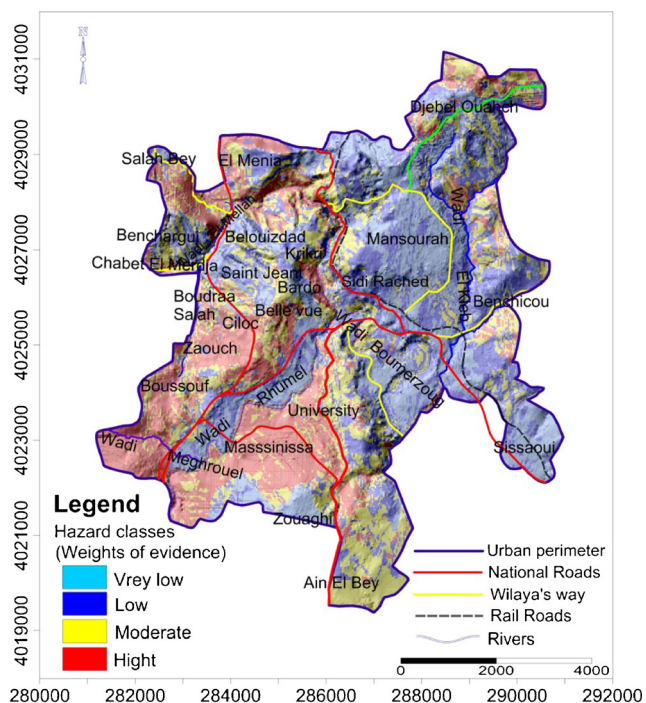
Fig. 9 Landslide hazard map obtained using the weights of evidence method

Fig. 10 Receiver operating characteristics (ROC) curves representing quality of the five models used

The ROC curve is one of the statistical techniques that can be used to provide predictions of the performance and to compare the different models (sensitivity vs. specificity). The area under ROC prediction curve (AUC) characterizes the quality of a forecast system by describing the system's ability to anticipate correctly the occurrence or nonoccurrence of a predefined "event" (Yesilnacar and Topal 2005; Chung and Fabbri 2003; Lee et al. 2003). The ROC curves can be summarized quantitatively based on the area under the ROC curve, which gives the accuracy of the developed model for predicting the landslide hazard. The quantitative–qualitative relationship between AUC and prediction accuracy can be given as follows: 0.9–1, excellent; 0.8–0.9, very good; 0.7–0.8, good; 0.6–0.7, average; and 0.5–0.6, poor (Yesilnacar and Topal 2005).

In this study, ROC curves have been obtained by comparing the landslide training pixels 30 % (2558 landslide pixels) with the six LHMs and the area under curves has been calculated. Figure 10 shows the ROC curves for the six landslide models. The validation results showed that the prediction accuracy of LHMs, produced by FR, WOE, AHP, Wf, Wi, and LR are, respectively, 86.59, 82.38, 77.86, 77.58, 76.77, and 70.45 %. The obtained results indicate that the use of FR for generating LSM provides more accurate prediction in comparison with WOE, AHP, Wf, Wi, and LR. Hence, it is concluded that all the employed models in this study show reasonably good accuracy in predicting the landslide hazard of the study area.

Also, the resulted LHMs have been verified using the two rules for spatial effective LHMs: First, the percentages of landslides increased concurrently with the degree of hazard
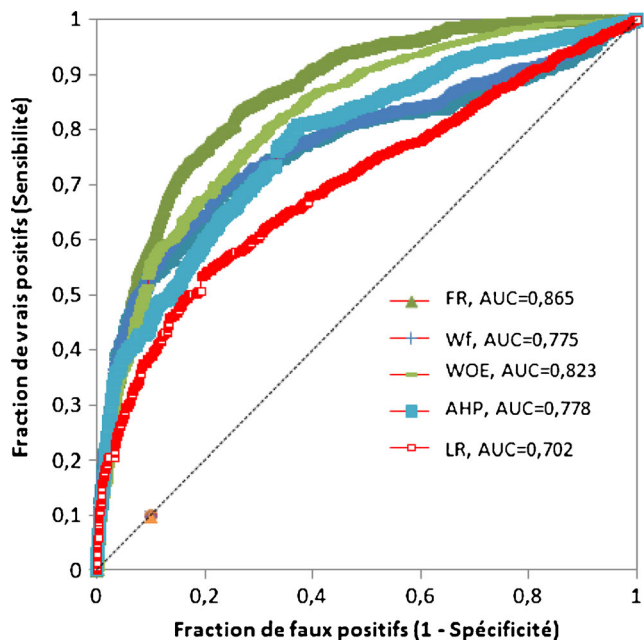
and the observed landslide should belong to the high hazard class, and second, the high hazard class should cover only small areas (Bai et al. 2010; Can et al. 2005; Pradhan and Lee 2010a; Pourghasemi et al. 2012c). The percentages of existing landslides falling into the four hazard classes have determined and presented in Table 9. It is deduced that the smaller amount of landslides was distributed in the low and very low hazard classes, and the higher amount of landslides were scattered in the high hazard class of the LHMs. Table 9 shows that the high hazard classes, found by using all the methods, contain 51 to 53 % of the active landslide zones, while the moderate zones give 26 % of the active landslide zones and about 13 % of the active landslide zones coincide within the moderate hazard class. The very low hazard zones show less than 7.5 % of the active landslide zones in all used methods. The results of Table 9 show that the percentages of landslides increase effectively from low to very high hazard and the high hazard class covers only small areas.

According to the obtained LHM from the FR model, 13 % of the total area falls in very low landslide hazard (Fig. 11). Low, moderate, and high hazard zones represent, respectively, 20, 17, and 13 % of the total area. In the established LHM with WOE model, 24 % of the total area belong to very low landslide hazard. Low and moderate hazard zones give, respectively, 26 and 25 % of the total area. While the high zones values give approximatively 24 %. The obtained LHM by using the AHP model shows 33.5 % of the total area in very low landslide hazard. Low, moderate, and high hazard zones give, respectively, 27, 20, and 19 % of the total area (Fig. 11). The produced LHM through the Wf method gives small percentages (13 %) for the high hazard areas, while the very low, low, and moderate

Table 9   Active landslide zones falling into the various classes of the landslide hazard maps

Methods	FR		LR		WOE		Wf		AHP	
Hazard classes	Total pixel	Area (%)	Total pixel	Area (%)	Total pixel	Area (%)	Total pixel	Area (%)	Total pixel	Area (%)
Very low	570	7.57	575	6.74	620	7.27	630	7.39	625	7.33
low	1158	15.38	1150	13.49	1170	13.72	1250	14.66	1160	13.61
Moderate	2298	26.96	2300	26.98	2355	27.62	2290	26.86	2350	27.57
Hight	4499	52.77	4500	52.79	4380	51.38	4355	51.09	4390	51.50

hazard areas are 22, 36, and 27 %, respectively. The LR method results are very low (40 %), low (28 %), moderate (21 %), and high (11 %). The high hazard zones percentages in the FR, AHP, Wf, and LR methods show small values of 13 % (Fig. 11), while the low hazard zones percentages in the FR, AHP, Wf, WOE, and LR methods show high values more than 25 %.

Discussion and conclusion

Landslides are among the most damaging natural hazards constituting a significant constraint for urban development in the Constantine city. Therefore, a landslide hazard map depicting the most vulnerable areas to landslides appears as a fundamental tool in risk management as an integral part of land use planning in the hazard prone areas. From scientific literature, various methods have been suggested for landslide hazard mapping, including heuristic, statistical, and deterministic based approaches. In recent years, several attempts have been made to apply different methods of LHM and to compare results in order to select the best suitable model.

In this research, we compare the obtained results of landslide hazard mapping by using five different methods: FR, Wf, LR, WOE, and AHP in the Constantine city, northeast of Algeria. The used methods are based on real, field-surveyed data, i.e., the spatial distribution of both landslides and/or the causal factors. Firstly, a landslide location has been identified by using aerial photographs and satellite images interpretation supported by available literature and field surveys. As a result, 70 % of

Fig. 11 Histograms showing the relative distribution of various hazard classes of different landslide hazard maps

identified landslides have been used as training data and the remaining (30 %) have been used to validate the models. Eight landslide-conditioning factors including lithology, slope gradient, slope exposure, land use, distance from roads, distance from streams, distance from faults, and precipitation have been considered for which to derive maps have been derived by using various GIS tools. The LHMs have been classified into five classes: very low, low, medium, and high using the standard deviation classifier. After that, the obtained LHM has been validated by comparison with known landslide locations.

According to the obtained area under the curve (AUC), the FR model showed higher prediction performance (86.59 %) than WOE (82.38 %), AHP (77.86 %), Wf (77.58 %), and LR (70.45 %) models. Hence, we concluded that all the employed models in this study give reasonably good accuracy in predicting landslide hazard for the Constantine city. Also, the accuracy results procedure by using statistics rules showed that the density of the landslides increases from low to very high hazard zone, and on the other hand, the high percentage of the landslides has been occurring in very high hazard area which covers the lower percentage the study area validating hence our results.

Such results have been observed in models such as FR, AHP, LR, and artificial neural network ANN (Yılmaz 2009; Pradhan and Lee 2010a; Park et al. 2012; Nourani et al. 2013); heuristic and bivariate statistical models, probabilistic, bivariate, and multivariate models (Pradhan and Youssef 2010; Tien Bui et al. 2011a; Kevin et al. 2011; Ozdemir and Altural 2012; Shahabi et al. 2012). Ayalew et al. (2005), Esmali Ouri, and Amirian (2009), through their works, stated that AHP model was better than the LR in Sado Island, Japan, and Iran, respectively. Yalcin (2008) reported that AHP method is a more realistic landslide susceptibility map than when using the bivariate statistical models (Wi and Wf). Also, Yalcin et al. (2011) found that the results of using the Wf method are better than the FR, AHP, Wi, and LR models in Trabzon, NE, Turkey. For landslide hazard analysis at Cameron area, Pradhan and Youssef (2010) showed that the FR model is provided better in predictions of landslides than bivariate and LR models. Yalcin (2008) evaluated the accuracy of the application of FR, LR, and ANN for landslide susceptibility mapping in the Ardesen (Turkey). The results showed that the AHP method provided realistic results of landslide
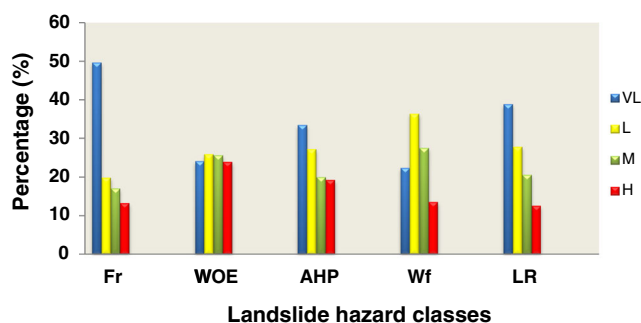
susceptibility than the Wi and Wf methods. Pourghasemi et al. (2013) presented the results of application of LR, SI, and AHP models for landslide susceptibility mapping in the north of Tehran metropolitan, Iran. The validation results indicated that the LR model is better in predictions of landslide susceptibility than using the SI and AHP models.

The resulted LHMs in this study may constitute a helpful tool for planners, decision makers, and engineers in slope management and future development planning in the city of Constantine. They may serve as useful guides for planners and engineers in choosing suitable locations for the implementation of developments. As the results are given at large scale, the exact extent of the slope instability areas and the details of high hazard area classes are determined, this will be useful for need further detailed site-specific studies. The area falling in the predicted high hazard zone is required to be monitored, and remedial and preventive measures may be initiated to protect life and property from future landslides. Also, it is worthy to mention that the same method can be used elsewhere in the northern part of Algeria where similar geological, geomorphological, and climatic feature prevails.

References

Aleotti P, Chowdhury R (1999) Landslide hazard assessment: summary review and new perspectives. Bull Eng Geol Environ 58:21–44

ARCADIS (2003) Etude des glissements de terrain de la ville de Constantine et de ses alentours. Unpublished report

Aris Y, Coiffait PE, Guiraud R (1998) Characterisation of Mesozoic–Cenozoic deformation and paleostress fields in the Central Constantinois, northeast Algeria. Tectonophysics 290:59–85

Atkinson PM, Massari R (1998) Generalized linear modelling of susceptibility to landsliding in the central Appennines, Italy. Comput Geosci 24(4):373–385

Ayalew L, Yamagishi H (2005) The application of GIS-based logistic regression for landslide susceptibility mapping in the Kakuda-Yahiko Mountains, Central Japan. Geomorphology 65:15–31

Ayalew L, Yamagishi H, Marui H, Kanno T (2005) Landslides in Sado Island of Japan: part II. GIS-based susceptibility mapping with comparison of results from two methods and verifications. Eng Geol 81: 432–445

Bai S, Wang J, Lu G, Zhou P, Hou S, Xu S (2010) GIS-based logistic regression for landslide susceptibility mapping of the Zhongxian segment in the three Gorges area, China. Geomorphology 115:23–31

Barbieri G, Cambuli P (2009) The weight of evidence statistical method in landslide susceptibility mapping of the Rio Pardu Valley (Sardinia, Italy). 18th World IMACS/MODSIM Congress, Cairns, Australia 13–17 July 2009

Barredo JI, Benavides A, Hervas J, Van Westen CJ (2000) Comparing heuristic landslide hazard assessment techniques using GIS in the Tirajana basin, Gran Canaria Island, Spain. Int JAppl Earth Obs Geoinf 2:9–23

Benaissa A, Bellouche MA (1999) Propriétés géotechniques de quelques formations géologiques propices aux glissements de terrain dans l'agglomération de Constantine (Algérie). Bull Eng Geol Environ 57:301–310

Bonham-Carter GF (1994) Geographic information systems for geoscientists: modeling with GIS. Pergamon Press, Ottawa, p 398

Bonham-Carter GF, Agterberg FP, Wright DF (1989) Weights of evidence modelling: a new approach to mapping mineral potential. In: Agterberg FP, Bonham-Carter GF (eds) Statistical applications in earth sciences. Geological Survey of Canada, Ottawa, pp 171–183

Bougdal R (2007) Urbanisation et mouvements de versants dans le contexte géologique et géotechnique des bassins néogènes d'Algérie du Nord. PhD thesis. USTHB, Algiers, p 185

Bougdal R, Belhai D, Antoine P (2006) Géologie de la ville de Constantine et de ses environs. Bull Serv Géol Algérie 18:3–23

Bourenane H, Bouhadad Y, Guettouche MS, Braham M (2014) GIS-based landslide susceptibility zonation using bivariate statistical and expert approaches in the city of Constantine (Northeast Algeria). Bull Eng Geol Environ. doi:10.1007/s10064-014-0616-6

Brabb EE (1984) Innovative approaches to landslide hazard and risk mapping. In: Proceedings of the fourth international symposium on landslides, vol 1. Canadian Geotechnical

Can T, Nefeslioglu HA, Gokceoglu C, Sonmez H, Duman TY (2005) Susceptibility assessments of shallow earthflows triggered by heavy rainfall at three subcatchments by logistic regression analyses. Geomorphology 72:250–271

Carrara A, Cardinali M, Guzzetti F, Reichenbach P (1995) GIS technology in mapping landslide hazard. In: Geographical information systems in assessing natural hazards. Kluwer, The Netherlands, pp 135–175

Cevik E, Topal T (2003) GIS-based landslide susceptibility mapping for a problematic segment of the natural gas pipeline, Hendek (Turkey). Environ Geol 44:949–962

Chung CJF, Fabbri AG (2003) Validation of spatial prediction models for landslide hazard mapping. Nat Hazards 30(3):451–472

Chung CJ, Fabbri AG (2008) Predicting landslides for risk analysis—spatial models tested by a cross validation procedure. Geomorphology 94:438–452. doi:10.1016/j.geomorph.2006.12.036

Crozier MJ, Glade T (2005) Landslide hazard and risk: issues, concepts and approach. In: Glade T, Anderson M, Crozier MJ (eds) Landslide hazard and risk. Wiley, Chichester, pp 1–40

Dai FC, Lee CF, Li JXu ZW (2001) Assessment of landslide susceptibility on the natural terrain of Lantau Island, Hong Kong. Environ Geol 40:381–391

Ercanoglu M, Gokceoglu C (2002) Assessment of landslide susceptibility for a landslide-prone area (North of Yenice, NW Turkey) by fuzzy approach. Environ Geol 41:720–730

Esmali Ouri A, Amirian S (2009) Landslide hazard zonation using MR and AHP methods and GIS techniques in Langan watershed, Ardabil, Iran. International Conference on ACRS 2009, Beijing, China

Gray DH, Leiser AT (1982) Biotechnical slope protection and erosion control. Van Nostrand Reinhold, New York

Guemache MA, Chatelain JL, Machane D, Benahmed S, Djadia L (2011) Failure of landslide stabilization measures: the Sidi Rached viaduct case (Constantine, Algeria). Afr Earth Sci pp 10 10.1016

Guiraud R (1973) Evolution post-triasique de l'avant-pays de la chaîne alpine en Algérie, d'après l'étude du bassin du Hodna et des régions voisines. PhD. thesis. Nice Univ

Guzzetti F, Carrara A, Cardinali M, Reichenbach P (1999) Landslide hazard evaluation: a review of current techniques and their application in a multi-scale study, Central Italy. Geomorphology 31:181–216

Isaaks EH, Srivastava RM (1989) An introduction to applied geostatistics. Oxford University Press, Oxford

Kevin LKW, Tay LT, Lateh H (2011) Landslide hazard mapping of Penang Island using probabilistic methods and logistic regression. Imaging Systems and Techniques (IST), 2011 I.E. International Conference, pp 273–278

Lee S, Min K (2001) Statistical analysis of landslide susceptibility at Yongin, Korea. Environ Geol 40:1095–1113

Lee S, Pradhan B (2007) Landslide hazard mapping at Selangor, Malaysia using frequency ratio and logistic regression models. Landslides 4:33–41

Lee S, Sambath T (2006) Landslide susceptibility mapping in the Damrei Romel area, Cambodia using frequency ratio and logistic regression models. Environ Geol 50(6):847–856

Lee S, Ryu JH, Lee MJ, Won JS (2003) Use of an artificial neural network for analysis of the susceptibility to landslides at Boun, Korea. Environ Geol 44:820–833

Leroi E (1996) Landslide hazard-risk maps at different scales: objectives, tools and development. In: Proc VII Int Symp Landslides, Trondheim, vol. 1. pp 35–52

Letouzey J, Tremolieres P (1980) Paleo-stress fields around the Mediterranean since the Mesozoic derived from microtectonics: comparison with plate tectonic data. Mém Bur Rech Géol Min 115:261–273

Machane D, Bouhadad Y, Cheikhlounis G, Chatelain JL, Oubaiche EH, Abbes K, Guillier B, Bensalem R (2008) Examples of geomorphologic and geological hazards in Algeria. Nat Hazards 45:295–308

Magliulo P, Di Lisio A, Russo F, Zelano A (2008) Geomorphology and landslide susceptibility assessment using GIS and bivariate statistics: a case study in southern Italy. Nat Hazards 47(3):411–435. doi:10.1007/s11069-008-9230-x

Nourani V, Komasi M, Alami M (2013) Geomorphology-based genetic programming approach for rainfall–runoff modeling. J Hydroinf 15(2):427–445

Ozdemir A, Altural T (2012) A comparative study of frequency ratio, weights of evidence and logistic regression methods for landslide susceptibility mapping: Sultan Mountains, SW Turkey. J Asian Earth Sci. doi:10.1016/j.jseaes.2012.12.014

Oztekin B, Topal T (2005) GIS-based detachment susceptibility analyses of a cut slope in limestone, Ankara-Turkey. Environ Geol 49(1):124–132. doi:10.1007/s00254-005-0071-6

Park S, Choi C, Kim B, Kim J (2012) Landslide susceptibility mapping using frequency ratio, analytic hierarchy process, logistic regression, and artificial neural network methods at the Inje area, Korea. Environ Earth Sci. doi:10.1007/s12665-012-1842-5

Pourghasemi HR, Pradhan B, Gokceoglu C (2012) Application of fuzzy logic and analytical hierarchy process (AHP) to landslide susceptibility mapping at Haraz watershed, Iran. Nat Hazards 63(2):965–996

Pourghasemi HR, Goli Jirandeh A, Pradhan B, Xu C, Gokceoglu C (2013) Landslide susceptibility mapping using support vector machine and GIS. J Earth Syst Sci 122(2):349–369

Pradhan B, Lee S (2009) Delineation of landslide hazard areas on Penang Island, Malaysia, by using frequency ratio, logistic regression, and artificial neural network models. J Environ Earth Sci (2010) 60:1037–1054. Doi: 10.1007/s12665-009-0245-8

Pradhan B, Lee S (2010) Delineation of landslide hazard areas using frequency ratio, logistic regression and artificial neural network model at Penang Island, Malaysia. Environ Earth Sci 60:1037–1054

Pradhan B, Youssef A (2010) Manifestation of remote sensing data and GIS on landslide hazard analysis using spatial-based statistical models. Arab J Geosci 3:319–326

RGPH (2008) 5ème Recensement de la Population et de l'Habitat en Algérie de l'Office National des Statistiques, (ONS, Avril 2008)

Saaty TL (1977) A scaling method for priorities in hierarchical structures. J Math Psychol 15:234–281

Saaty TL (1980) The analytical hierarchy process. McGraw Hill, New York

Saaty TL (2008) Decision making with the analytic hierarchy process. Int J Serv Sci 1(1):83–98

Shahabi H, Ahmad BB, Khezri S (2012) Evaluation and comparison of bivariate and multivariate statistical methods for landslide susceptibility mapping (case study: Zab basin). Arab J Geosci. doi:10.1007/s12517-012-0650-2

Soeters R, Van Westen CJ (1996) Slope instability recognition, analysis, and zonation. In: Turner KA, Schuster RL (eds) Landslides: investigation and mitigation. Transport Research Board Special Report, vol 247. pp 129–177

Suzen ML, Doyuran V (2004) Data driven bivariate susceptibility assessment using geographical information systems: a method and application to Asatsuyu catchment, Turkey. Eng Geol 71:303–321

Thiery Y, Malet JP, Sterlacchini S, Puissant A, Maquaire O (2007) Landslide susceptibility assessment by bivariate methods at large scales: application to a complex mountainous environment. Geomorphology 92:38–59. doi:10.1016/j.geomorph.2007.02.020

Tien Bui D, Lofman O, Revhaug I, Dick O (2011) Landslide susceptibility analysis in the Hoa Binh province of Vietnam using statistical index and logistic regression. Nat Hazards 59:1413–1444

Van den Eeckhaut M, Vanwalleghem T, Poesen J, Govers G, Verstraeten G, Vandekerckhove L (2006) Prediction of landslide susceptibility using rare events logistic regression: a case-study in the Flemish Ardennes (Belgium). Geomorphology 76:392–410

Van Westen CJ (1993) Application of geographic information systems to landslide hazard zonation. ITC publication, vol. 15. International Institute for Aerospace and Earth Resources Survey, Enschede, p 245

Van Westen CJ (1997) Statistical landslide hazard analysis. ILWIS 2.1 for windows application guide. ITC publication, Enschede, pp 73–84

Van Westen CJ, Rengers N, Terlien MTJ, Soeters R (1997) Prediction of the occurrence of slope instability phenomena through GIS-based hazard zonation. Geol Rundsch 86(2):404–414

Van Westen CJ, Rengers N, Soeters R (2003) Use of geomorphological information in indirect landslide susceptibility assessment. Nat Hazards 30:399–419

Vargas LG (1990) An overview of the analytic hierarchy process and its applications. Eur J Oper Res 48:2–8

Varnes DJ (1978) Slope movement, types and processes. In: Schuster RL, Krizek RJ (Eds) Landslides, analyses and control. National Academy of Science, Report 176, Washington, DC, pp 11–35

Varnes DJ (1984) Landslide hazard zonation, a review of principles and practice. IAEG Commission on Landslides. UNESCO, Paris. 63 pp

Vila JM (1980) La chaîne alpine d'Algérie orientale et des confins algéro-tunisiens. Ph.D thesis. Paris VI Univ

Yalcin A (2008) GIS-based landslide susceptibility mapping using analytical hierarchy process and bivariate statistics in Ardesen (Turkey): comparisons of results and confirmations. Catena 72(1):1–12. doi:10.1016/j.catena.2007.01.003

Yalcin A, Reis S, Aydinoglu AC, Yomralioglu T (2011) A GIS-based comparative study of frequency ratio, analytical hierarchy process, bivariate statistics and logistics regression methods for landslide susceptibility mapping in Trabzon, NE Turkey. Catena 85:274–287

Yesilnacar E, Topal T (2005) Landslide susceptibility mapping: a comparison of logistic regression and neural networks methods in a medium scale study, Hendek region (Turkey). Eng Geol 79(3–4):251–266. doi:10.1016/j.enggeo.2005.02.002

Yılmaz I (2009) Landslide susceptibility mapping using frequency ratio, logistic regression, artificial neural networks and their comparison: a case study from Kat landslides (Tokat-Turkey). Comput Geosci 35(6):1125–1138

Zhou G, Esaki T, Mitani Y, Xie M, Mori J (2003) Spatial probabilistic modeling of slope failure using an integrated GIS Monte Carlo simulation approach. Eng Geol 68:373–386